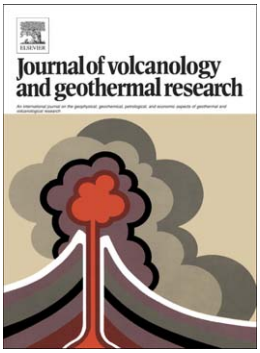

Olivine-Hosted Glass Inclusions from Scoriae Erupted in 1954–2000 at Mount Cameroon Volcano, West Africa

C.E. Suh, J.F. Luhr, M.S. Njome

PII: S0377-0273(07)00221-1
DOI: doi: 10.1016/j.jvolgeores.2007.07.004
Reference: VOLGEO 3718

To appear in: *Journal of Volcanology and Geothermal Research*

Received date: 15 January 2007
Revised date: 19 July 2007
Accepted date: 20 July 2007

Please cite this article as: Suh, C.E., Luhr, J.F., Njome, M.S., Olivine-Hosted Glass Inclusions from Scoriae Erupted in 1954–2000 at Mount Cameroon Volcano, West Africa, *Journal of Volcanology and Geothermal Research* (2007), doi: 10.1016/j.jvolgeores.2007.07.004

Olivine-Hosted Glass Inclusions from Scoriae Erupted in 1954-2000 at Mount Cameroon Volcano, West Africa

C.E. Suh[1*], J.F. Luhr[2╬§], and M.S. Njome[1]

1 – Economic Geology Unit, Department of Geology and Environmental Science, University of Buea, P.O. Box 63, Buea, South West Province, Cameroon.

2 - Department of Mineral Sciences, National Museum of Natural History, P.O. Box 37012, NHB-119, Smithsonian Institution, Washington DC 20013-7012, USA.

* Corresponding author
╬ Deceased
§ Paper dedicated to the memory of Jim Luhr as a tribute to his immense contribution to Volcanology especially in developing countries.

Email addresses: CES: chuhma@yahoo.com; MSN: mnjome@yahoo.com

Abstract

Concentrations of major, trace, and volatile elements are reported for olivine-hosted glass inclusions from intraplate-type, *nepheline*-normative trachybasaltic to basanitic scoria samples representing five historical eruptions (1954, 1959, 1982, 1999, and 2000) of Mount Cameroon (4.20^{o}N, 9.17^{o}E). Bulk-rock and mineral compositions are also reported for the same scoria samples and for lava samples from the same eruptions. Mineral analyses are also presented for a spinel-harzburgite mantle xenolith, which we suggest may be the youngest (and freshest) mantle sample known. Mount Cameroon magmas have eruption temperatures of 1,150-1,200^{o}C and have relatively high oxygen fugacities just above the trend of the synthetic Ni-NiO buffer. The most-primitive glass inclusion analyzed is also the most volatile-rich, with 1.7 wt% H_2O, 967 ppm CO_2, 1,530 ppm F, 2,400 ppm S, and 1,270 ppm Cl. The Mount Cameroon F contents are the highest known for basaltic glasses. The relatively high CO_2 contents in Mount Cameroon glass inclusions supports the interpretation that the CO_2 gas responsible for the Lakes Monoun and Nyos gas disasters is magmatic in origin.

Introduction

Recent compositional studies of glass inclusions trapped and quenched in host phenocryst minerals have led to improved understanding of the petrogenesis of basaltic magmas, parental magma diversity, and pre-eruptive melt volatile contents (Sisson and Layne, 1993; Vogel and Aines, 1996; Roggensack et al., 1997; Sisson and Bronto, 1998; Dixon and Clague, 2001; Luhr, 2001; Danyushevsky et al., 2002; Hauri, 2002; Norman et al., 2002, 2004; Sours-Page et al., 2002; Cervantes and Wallace, 2003; Métrich et al., 2004; Gurenko et al., 2005; Saito et al., 2005; and other publications cited later). Glass inclusions provide insights into the chemical compositions of the melt phase at various crustal depths of entrapment, even extending upward into the dynamic volcanic conduit region (Blundy et al., 2006). Magma degassing is an important theme for volcanological research because this process not only affects the onset and path of magmatic crystallization but also influences the explosivity of eruptions. Volcanoes that erupt frequently, such as Mount Cameroon, provide an opportunity for comparing the compositions of glass inclusions erupted at different times.

This paper examines glass inclusions in olivine crystals separated from cm-sized scoriae from five historical eruptions of Mount Cameroon (1954, 1959, 1982, 1999, and 2000), and bulk-rock compositions of those 5 tephra samples and 11 lava samples from the same eruptions. The main aims are to: (i) determine concentrations of the main volatile species and derived parameters ($H_2O^{molecular}$, OH^-, H_2O^{total}, CO_3^{2-}, F, Cl, SO_3^{total}, and S^{6+}/S^{2-}) in the olivine-hosted glass inclusions, (ii) investigate the diversity

represented by bulk-rock and glass compositions, (iii) estimate pre-eruptive temperature, pressure, and oxygen fugacity for these magmas, and (iv). assess the importance of degassing by Mount Cameroon magmas prior to eruption. Data on the volatile contents of Mount Cameroon magmas are particularly important because the volcano lies along the same volcanic chain as Lakes Nyos and Monoun, where catastrophic releases of toxic volcanic gases rich in CO_2 in 1985 and 1986, respectively, killed over 1,800 people (see papers in Le Guern and Sigvaldason, 1989).

Geological Setting

Mount Cameroon is a large stratovolcano with an estimated volume of ~1,200 km^3, part of the ~1,600 km long alignment of volcanoes termed the Cameroon volcanic line (Fig. 1; CVL hereafter). The CVL has been extensively discussed in the literature (see Fitton and Dunlop, 1985; Aka et al., 2004; Rankenburg et al., 2004a, 2004b, and older references therein). The CVL runs SW-NE following a major left-lateral fault system that extends from the Atlantic Ocean into west-central Africa. There is no evidence for a systematic shift in the focus of volcanism along the CVL with time, and consequently its origin cannot be explained by a single static mantle hotspot with the African plate passively gliding over it (Fitton and Dunlop, 1985; Marzoli et al., 1999). CVL volcanoes have erupted a wide variety of alkaline rocks since ~31 Ma (Ngounouno et al., 2004). The interested reader is referred to the references cited above for full discussions on CVL tectonics and magmagenesis.

Mount Cameroon lies just landward (centered ~25 km east) of the ocean/continent

boundary of the CVL (Fig. 2). Rising to 4,095 m, it marks the highest peak along the CVL and has erupted eight times since the start of the last century (1909, 1922, 1925, 1954, 1959, 1982, 1999, and 2000). The only other CVL volcanoes with known AD eruptions are Lake Nyos, with a radiocarbon-dated eruption at 1550 AD, and Santa Isabel volcano on the Atlantic Island of Bioko, with known eruptions in 1903 and 1923 (Siebert and Simkin, 2002). Details of the recent eruptions of Mount Cameroon are reported elsewhere (Geze, 1953; Fitton et al., 1983; Venzke et al., 2002; Suh et al., 2003). Most eruptions have two vent systems: (i) fissures at higher altitudes characterized by weak Strombolian fire fountaining, and (ii) flank vents also along fissures, at lower elevations typified by Hawaiian-style effusive activity. Accordingly, construction of pyroclastic cones dominates at the higher vent systems, while lava emission is preponderant at lower vents (Suh et al., 2003 & 2005).

Previous Petrological and Geochemical Studies

The most important modern petrological and geochemical studies of Mount Cameroon volcanic rocks are reported in Fitton et al. (1983), Déruelle et al (1987), Halliday et al. (1990), Sato et al. (1990), and Suh et al. (2003). These authors have used a variety of terms to describe the Mount Cameroon rocks, including basalt, basanite, tephrite, hawaiite, picrite, and ankaramite. All of the bulk-rock analyses from these papers, plus those from this study (Table 2), are plotted on the Total Alkalies vs Silica (TAS) diagram in Fig. 3; they range in SiO_2 from 42.0 to 52.5 wt%. All of these samples have *nepheline* in the CIPW norm. The historical samples from this study (Table 2:

1954-2000 eruptions) straddle the basanite-trachybasalt boundary, as do other historical samples from Fitton et al. (1983) and Suh et al. (2003). Studies that also considered pre-historical products of Mount Cameroon have reported somewhat more diverse bulk-rock compositions, which also spill into the TAS fields of basalt, phonotephrite, and basaltic trachyandesite (Fig. 3). These studies have clearly established that Mount Cameroon magmas are of intraplate type, with characteristically high concentrations of the high-field-strength elements Ti, Nb, and Ta.

Déruelle et al. (1987) argued that fractional crystallization of olivine, clinopyroxene, and Fe-Ti oxides is the dominant process controlling the overall differentiation of the Mount Cameroon magma suite. Fitton et al. (1983), however, noted the inadequacy of fractional crystallization to model the minor compositional variations observed in the 1982 eruption, which they found to be best explained by mixing between the final (and most mafic) 1982 magma composition and magma similar to the 1959 lava. This view was supported by Suh et al. (2003 & 2005), who demonstrated that the lavas from different historical eruptions have subtle geochemical differences, indicating that they represent pockets of magma that differentiated in slightly different ways prior to eruption. They inferred that the volcano does not have a single, periodically replenished, and continuously fractionated magma reservoir, but rather a system of many small-volume magma-storage regions in which distinct magma batches may evolve and erupt independently, or may first mingle and mix with other similar but compositionally distinct magma batches, or with residual magma from previous eruptions.

Sample preparation and analytical methods

Small scoria fragments (1-3 cm in diameter) were collected from each of the tephra deposits of the 1954, 1959, 1982, 1999, and 2000 eruptions, at their higher altitude vent system. All 5 tephra samples are fresh.. Eleven lava samples were collected from lava flows at the lower altitude vent system of four (1959, 1982, 1999, 2000) of these same eruptions. The 1954 eruption produced only tephra without lava. A single spinel-harzburgite xenolith, 8 cm x 6 cm x 4 cm in size with a thin lava coating was collected at the upper vent of the 2000 eruption. This is arguably the youngest and most pristine ultramafic xenolith on Earth. Sample locations are listed in Table 1 and shown on Fig. 2.

Modes for the 16 volcanic samples and for the peridotite xenolith were determined by point counting of polished thin sections (Table 1). A portion of each scoria and lava sample was crushed in an alumina-plated jaw crusher and then pulverized in a shatterbox with an alumina container and puck. These powders were analyzed for major and trace elements by X-ray fluorescence (XRF) spectroscopy at the Smithsonian Institution, where we also measured loss on ignition and FeO concentrations by potassium-dichromate titration. The same rock powders were analyzed for additional trace elements at Washington State University by inductively coupled plasma mass spectrometry (ICP-MS). These bulk-rock analyses are listed in Table 2. Luhr and Haldar (2005) presented details of the XRF methodology and gave precision and accuracy evaluations for both the Smithsonian XRF and the Washington State University ICP-MS laboratories.

Olivine crystals with glass inclusions were separated from each of the 5 scoria samples. Portions of these scoria samples were gently crushed and sieved, and the 0.335 mm to 0.5 mm size-fraction was used for olivine separation, selection, and preparation following techniques described in Luhr (2001). The petrographic descriptions of the 26 analyzed glass inclusions are given in Table 5. Only glass inclusions >20 microns in each dimension were selected for investigation. Based on this size criterion, several olivine crystals were separated and processed but most of these turned out to be unsuitable for analyses (when viewed under the SEM) thereby greatly reducing the number of glass inclusions analyses reported in this study. These unsuitable inclusions showed various degrees of devitrification, leakage and extensive post-entrapment crystallization of olivine. Thus, despite the fact that the glass inclusions analysed for each eruption are not so many, these rigorous selection criteria ensured that the results reported here can be interpreted as being truly representative of the composition of melt inclusions at this volcano.

Mineral and glass compositions were analyzed using the Smithsonian's JEOL-8900 electron microprobe, following analytical techniques discussed in Luhr and Haldar (2005). Compositions of intergrown olivine and clinopyroxene crystals across sharp contacts, used for estimation of magmatic temperature following Loucks (1996), are given in Table 3. Average compositions of mineral cores in the spinel-lherzolite xenolith are listed in Table 4. Major elements, total sulphur (as SO_3^t) and Cl in glass inclusions, and compositions of adjacent host olivine were determined by electron microprobe (Table 6). In order to evaluate the oxidation state of S in Mount Cameroon samples

(%S^{6+}, Table 6), electron-microprobe S-K∀ peak positions for each glass inclusion were evaluated against those for troilite (pure S^{2-}) and anhydrite (pure S^{6+}) (see Luhr, 2001 for details) following methods described by Carroll and Rutherford (1988), Nilsson and Peach (1993), Wallace and Carmichael (1994), Metrich and Clocchiatti (1996), Matthews et al. (1999), and Jugo et al. (2005).

In four of the glass inclusions, concentrations of hydrogen and carbon species ($H_2O^{molecular}$, OH^-, H_2O^{total}, CO_3^{2-}) were measured by transmission Fourier-transform infrared (FTIR) spectroscopy on doubly polished wafers at the Smithsonian (Table 9) following analytical procedures described in Luhr and Haldar (2005). The bulk-rock powder of Mount Cameroon basanite scoria sample (SI2000/5), devolatilized in a 1-atm furnace at 1330°C with oxygen fugacity equivalent to the synthetic Ni-NiO buffer (Huebner and Sato, 1970), was used as a background reference sample for the carbonate peaks 1515 cm^{-1} and 1435 cm^{-1}. These FTIR background corrections were performed with a least-squares peak-fitting routine written by Sally Newman (pers. comm.) using the Solver tool in Excel, to subtract the spectrum of the devolatilized glass from that of the glass inclusion. Three of the four glass inclusions analyzed by FTIR were also analyzed for H_2O, CO_2, F, S, and Cl by secondary-ion mass spectrometry (SIMS) using the Carnegie Institution ion microprobe following techniques described in Hauri et al. (2002) and Luhr and Haldar (2005), with data listed in Table 8. Finally, three of the four glass inclusions analyzed by FTIR were analyzed for 27 elements by laser-ablation inductively coupled plasma mass spectrometry (LA-ICP-MS) at the University of Maryland following the method of Michael et al. (2002), with data and precision

estimates listed in Table 7.

Results and interpretations

Bulk-Rock Compositions

As seen in the multi-element "spider" diagram of Fig. 4A and the companion REE diagram of Fig. 4B, the analyzed volcanic rocks from 1954-2000 eruptions of Mount Cameroon are geochemically similar. These diagrams also show that the Mount Cameroon rocks are typical of the Ti-Nb-Ta-rich, *ne*-normative, intraplate-type basanites known worldwide as seen in comparisons with similar volcanic rocks from the Azores, Canary Islands, Hawaii, and Mexico.

On SiO_2-variation diagrams, the major and trace elements fall cleanly into two groups: (1) with compatible behaviour, decreasing with increasing silica (Ti, Fe, Mg, Ca, Sc, V, Cr, Co, Ni, Cu, and Zn), and (2) with incompatible behaviour, increasing with silica (Al, Na, K, P, Rb, Sr, Y, Zr, Nb, Cs, Ba, La, Ce, Pr, Nd, Sm, Eu, Gd, Tb, Dy, Ho, Er, Tm, Yb, Lu, Hf, Ta, Pb, Th, and U). These trends are consistent with control by fractional crystallization of olivine, clinopyroxene, and titanomagnetite, as previously noted by Déruelle et al. (1987).

Three compatible and three incompatible elements are plotted versus SiO_2 in Fig. 5, with regression coefficients (R^2) that range from 0.96 to 0.84. These deviations from perfect correlation probably indicate some variability in the fractional crystallization process at Mount Cameroon. On trace element binary diagrams, negative correlations exist between the very compatible elements (e.g. Sc, Co) and the highly incompatible

element Nb (Fig. 5G and H). Conversely, positive correlations are discernible between the incompatible elements (e.g. Ba, Rb, Zr) and Nb (Fig. 5I, J, and K). These trends appear to be coherent with a history of magma differentiation through fractional crystallization of the main phenocryst phases in the scoriae and lavas. Indication of small but significant distinctions in the compositions of historical magma batches, however, is evident on a plot of the incompatible element Th versus Nb/Ta (Fig. 6A), the ratio of two high-field-strength elements that are not expected to fractionate during most magmatic processes, and the companion plot of MgO versus Nb/Zr (Fig. 6B). Scoria and lava samples from the different historical eruptions plot in distinct positions on these diagrams, with those erupted in 1959, 1982, and 1954-2000 clustered fairly tightly, and the 1999 samples partially overlapping the other fields. If the scoria and lava from the various eruptions evolved along a liquid line of descent from a common parental magma through fractional crystallization alone, then the trace element ratios such as Nb/Zr should vary systematically with an established index of magma differentiation such as MgO content. From Figure 6B it is observed that there is a significant rise in Nb/Zr ratio in the 1982 samples accompanied by only a very small drop in MgO content. It is clear from this plot that the 1982 magma resulted from mixing of slightly different magma batches. Therefore, the small variations in the incompatible element ratios support the notion of small, magma batches beneath Mount Cameroon, each of which evolves thermally and by fractional crystallization, according to its particular ascent history.

Petrography and Mineral Compositions

Scoriae from the 1954 eruption are the richest in olivine phenocrysts (Table 1: 7.7 vol %), a few of which reach 2 mm in size. These phenocrysts are typically euhedral, isolated, and have spherical glass inclusions. A few olivine phenocrysts were observed to be surrounded by coronae of titanomagnetite. Ten analyzed olivine crystals immediately adjacent to clinopyroxene crystals are very homogeneous (Table 3: $Fo_{77.8-78.9}$), but poorer in MgO than all but one of five analyzed olivine adjacent glass inclusions (Table 6: $Fo_{78.4-83.9}$). Clinopyroxene phenocrysts reach 1.5 mm in size and commonly show compositional zoning and resorbed margins. Aggregates of clinopyroxene + olivine + plagioclase $\pm$ titanomagnetite are common and the clinopyroxene in these aggregates is characteristically anhedral. Olivine phenocrysts can be partially enclosed by clinopyroxene, evidence of the sequence of crystallization. Analyzed clinopyroxene immediately adjacent to olivine are also compositionally homogeneous (Table 3: $Wo_{50}En_{39}Fs_{11}$). Plagioclase phenocrysts commonly reach lengths of 1 mm. The groundmass has light-brown glass studded with microlites of the same four minerals present in the aggregates.

In contrast, the 1959 scoria sample has <1% of olivine phenocrysts (Table 1), the lowest among the analyzed tephra, consistent with having the lowest bulk-rock MgO content (Table 2). The observed olivine microphenocrysts are fragmented and typically have convoluted and resorbed margins, with compositions similar to those for the 1954 scoriae. Clinopyroxene crystals are compositionally zoned, subhedral to euhedral in form, and rich in opaque inclusions. Analyzed clinopyroxenes immediately adjacent olivines are considerably poorer in MgO compared to the 1954 scoriae (Table 3:

$Wo_{51}En_{33}Fs_{16}$). Plagioclase exists as both phenocrysts and microphenocrysts and is the dominant microlite phase in the groundmass.

The 1982 scoria sample is the most aphyric of the suite, with the groundmass accounting for 90 vol.% (Table 1). Plagioclase and titanomagnetite only exist as microlites in the groundmass. Isolated olivine phenocrysts are similar in composition to those from the 1954 scoriae, but they and the olivine microphenocrysts are subhedral and have irregular, serrated, jagged, and convoluted margins. Most are so extensively resorbed from rim to core that only an outline of the once-subhedral crystal is preserved. Clinopyroxene phenocrysts are pale green, typically euhedral, and found in clusters. Isolated crystals are larger (reaching ~0.7 mm) with much greener (Fe-rich) rims. The analyzed clinopyroxenes adjacent to olivine are very similar in composition to those from the 1959 scoriae (Table 3). The matrix is glassy with numerous randomly oriented, needle-shaped microlites.

The scoria samples from the 1999 and 2000 eruptions are both porphyritic, but the 1999 sample has more olivine and less clinopyroxene phenocrysts than the 2000 sample (Table 1). Olivine phenocrysts are fragmented and range from 0.4 mm to ~2 mm in size. Analyzed olivine crystals adjacent clinopyroxene are the most Mg-rich of the suite (Table 3: $Fo_{83.7\text{-}85.4}$). In contrast, compositions of host olivine adjacent glass inclusions are similar to those from other samples (Table 6: $Fo_{77.6\text{-}82.2}$). Clinopyroxene compositions are intermediate to those reported for other samples.

The lava samples from these eruptions have similar modes (Table 2) and mineralogical characteristics to the corresponding tephra. Their textures were described

in Suh et al. (2003).

The peridotite xenolith recovered from the 2000 pyroclastic deposit has a coarse-equant texture (Harte, 1977) and contains olivine, orthopyroxene, clinopyroxene, and spinel (Table 1); thus it classifies as a spinel harzburgite. The Mg# (100xMg/(Mg+Fe)) of olivine and pyroxenes are ∃90 (Table 4), significantly higher than those for olivine and clinopyroxene phenocrysts in the Mount Cameroon volcanic rocks (Tables 3 and 6), but typical of mantle xenoliths. The mineral chemistry of this xenolith is similar to that of xenoliths from other volcanoes along the CVL (e.g. Princivalle et al., 2000). Previous studies at Mount Cameroon volcano have identified xenocrysts in the lava samples interpreted to represent entrained fragments from intrusions disrupted by ascending magma (Suh et al. 2003). These xenocrysts include olivine (Fo_{83-85}) and clinopyroxene (Mg#: 75 – 76), with mg #s significantly lower than those for the xenolith minerals yet slightly higher than those for the pristine phenocryt phases in the volcanic rocks. The mineral composition of the peridotite xenolith presented here, considering the paucity of data on mantle pieces at Mount Cameroon volcano, are therefore useful in distinguishing between entrained mineral fragments (xenocrysts), pristine phenocrysts, and remnants of mantle rocks in eruptive products of this volcano.

Glass Inclusions: Morphology and Compositions

Glass inclusions in recent Mount Cameroon scoriae have a wide range of sizes and shapes (Table 5 and Fig. 7). Most of the analyzed inclusions are over 50 :m across and roughly spherical in shape (Fig. 7a) whereas others have lensoid (Fig. 7b, c) or

irregular shapes (Fig. 7d). The larger inclusions have spherical vapor bubbles ~10-45 :m across, which represent ~1-16 % of the glass-inclusion volumes (Table 5). The glass inclusions also commonly contain inclusions of subhedral to euhedral spinel (Fig. 5a) and can have tiny spherical sulphide grains usually < 10 :m in size. These sulphide grains are usually too small to be analyzed by EMP. However EDS patterns indicated Fe-Ni-S-Cu peaks.

Electron-microprobe analyses of glass inclusions from Mount Cameroon scoriae are presented in Table 6, along with glass compositions corrected for precipitation of olivine onto the inclusion walls following the methodology discussed in Luhr (2001). The estimated amounts of precipitated olivine ranged from 0 to 8 wt.% and averaged 5 wt.%.

Comparisons of corrected glass-inclusion compositions and bulk-rock compositions are shown in Fig. 8. Most glass compositions either conform to the same trend as the bulk-rock compositions (Fig. 8A: SiO_2 versus K_2O), or form a sub-parallel trend (Fig. 8B: SiO_2 versus CaO). The most notable exceptions are the 5 analyzed glass inclusions from the 1954 eruption, which scatter all across these plots. The 1954 glasses also have among the highest EMP totals (Fig. 8C), taken to signify low H_2O values, and are hosted by olivines with among the highest Mg#s (100xMg/(Mg+Fe)) in the suite (Fig. 8D). At the other extreme are samples from the 1982 eruption, for which the bulk-rock and glass compositions show considerable similarity and overlap (Figs 8A and B); this is true to a somewhat lesser degree for the 2000 eruption.

The plot of SiO_2 versus SO_3^{total} in Fig. 9A shows an overall negative trend, similar

to those observed in many other glass-inclusion studies (Luhr, 2001; Métrich et al., 2001 & 2004; Wade et al., 2006) and interpreted as evidence for degassing during differentiation and ascent. When viewed eruption by eruption, however, only the 5 glass inclusions from the 1954 eruption show such behavior and define the overall trend. Glass inclusions for the other samples form clusters along the overall trend, with the 3 inclusions from the 1959 eruption and one from the 1982 eruption marking the high-S, low-SiO_2 end of the trend. These 4 glass inclusions, therefore, provide the best estimate of the primitive glass compositions for Mount Cameroon. One of these primitive glass inclusions (59-1A) was among the 4 analyzed for trace elements by LA-ICP-MS (Table 8). Cl contents of the glass inclusions show little variation with SiO_2 (Fig. 9C), but do show an overall positive correlation with P_2O_5 (Fig. 9D), K_2O, and presumably all other incompatible elements in these magmas. Considering all the melt inclusions, P_2O_5 and K_2O also seem to define positive correlation (Fig. 9E). As discussed for Fig. 9A, however, the majority of this trend is defined by the highly variable 1954 glasses. In contrast, SO_3^{total} shows no correlation with P_2O_5 (Fig. 9B), consistent with a higher vapor/melt partition coefficient for S considerably greater than that for Cl (Carroll and Webster, 1994; Scaillet et al., 1998; Keppler, 1999; Spilliaert et l., 2006). Compositional modification of melt inclusions in a host olivine (e.g. through crystallization) does not affect the CaO/Al_2O_3 and Na_2O/TiO_2 ratios of melt inclusions. (Gioncada et al., 1998; Norman et al., 2002). These ratios (Fig. 9F) therefore are unrelated to post entrapment modification but reflect the compositional characteristics of the parental magma represented by the melt inclusion. The Mount Cameroon melt inclusions span a broad

range in CaO/Al_2O_3 ratios (Fig. 9F) with slight differences among the melt inclusions from the different eruptions. The variation shown in Fig. 9F cannot be explained by simple fractional crystallization from a single homogenous melt as described by Gioncada et al. (1998; their Fig. 5) but requires some degree of mixing of liquids (especially for the 1954 inclusions) at various stages of evolution (Norman et al., 2002).

Concentrations of 24 trace elements in three Mount Cameroon glass inclusions determined by LA-ICP-MS are listed on Table 8 and multi-element and REE plots showing these data in comparison to bulk-rock ICP-MS data are shown in Figs. 10A and B. The glass inclusion compositions are completely enveloped by the bulk-rock values, with the minor exceptions of several middle and heavy REE values.

Most glass inclusions have total S (SO_3^t) values above 0.4 wt.%, with the highest values of 0.71 wt.% for two 1959 inclusions (Table 6). These 1959 melt inclusions also show high CaO content with K_2O/P_2O_5 ratios (Fig. 9E) that do not change significantly. This could suggest that their high S concentrations could be related to crystallization. However, spherical sulfide blebs were encountered in the 1959 inclusions, indicating that these melts were sulfide saturated (e.g. Davis et al., 2003). Estimates of $\%S^{6+}$ in the glass inclusions derived from electron-microprobe peak position measurements are listed in Table 6. Although some low outliers exist, particularly in 1954 glasses, the majority of the glass inclusions yielded $\%S^{6+}$ values of 20-50, with a mean of 31 $\forall$ 15.

Only four glass inclusions were analyzed for volatile components by FTIR, and only three of these were analyzed for volatiles by SIMS (Table 7). H_2O contents by SIMS are consistent at ~1.7 wt.%, somewhat higher than those by FTIR (~1.2 wt.%). We

prefer the SIMS values as the technique shows little compositional dependence of the calibration for basalts (Hauri et al., 2002), whereas FTIR absorption coefficients are not well established for basanitic glasses. The SIMS H_2O measurements were made against natural basaltic glasses. However, the FTIR data, if considered as reliable by ignoring the uncertainties in the extinction coefficients of the standards used, provide a reliable lower limit for the H_2O content in Mount Cameroon magmas. The SIMS and FTIR data show better consistency for CO_2, with SIMS values of 683-967 ppm. SIMS F values range 1,530-1,982 ppm. A considerable discrepancy exists between S values by SIMS (2,619-3,096 ppm) and those by EMP (1,882-2,411 ppm), with the former up to 50% higher than the latter. The SIMS data are calibrated against various natural glasses (Hauri et al., 2002), whereas the EMP analyses are calibrated against the Smithsonian scapolite standard (Jarosewich et al. 1980), and this apparent discrepancy appears to reflect an unresolved inconsistency in these two calibrations. We have observed the same apparent discrepancy between these two techniques for other glass suites although it could simply be due to the scapolite standard used for the EMP calibration resulting in the underestimation of S in the melt inclusions analyzed by electron probe (Metrich, personal communication, 2007). Cl values by SIMS (983-1,070 ppm) and EMP (980-1,270 ppm), calibrated in the same manner as for S, show considerably greater consistency.

Discussion

Pre-eruptive Magma Conditions: T, P, and fO_2 Estimates

We evaluated two different geothermometers for Mount Cameroon's historical

magmas. Co-existing olivine/clinopyroxene pairs in contact across clean phenocryst or microphenocryst interfaces allowed for the calculation of equilibrium crystallization temperatures following the method of Loucks (1996) as listed in Table 3. Equilibration temperatures were also calculated from the MgO contents of the olivine-hosted and olivine-corrected glass-inclusion compositions following Sugawara (2000) as listed in Table 6. These temperature estimates are plotted versus eruption year in Fig. 11A. The olivine/clinopyroxene temperatures (n=35) have mean and 1Φ values of 1,206 ∀ 66°C, systematically higher than the glass-inclusion temperatures (n=26: 1,148 ∀ 16°C). Within the inherent uncertainties of these two methods, pre-eruptive temperatures for recent Mount Cameroon magmas were likely in the range 1,150-1,200°C, with those for 1954 apparently at the low end of the range.

We also evaluated two different methods for estimating magmatic oxygen fugacities. First we used the method of Kress and Carmichael (1991) based on measured Fe_2O_3 and FeO values in bulk-rock samples. These are listed in Table 2 as)NNO values, in log units relative to the synthetic Ni-NiO buffer (Huebner and Sato, 1970); all of these bulk-rock samples were analyzed for bivalent Fe by potassium-dichromate titration (Peck, 1964), for total Fe as FeO by XRF, and for Fe_2O_3 by difference. Rhodes and Vollinger (2005) emphasized the importance of the quench history of each sample in the evaluation of oxygen fugacity by this approach, with the most rapidly quenched and least-altered samples recording the lowest values. For subaerial eruptions, virtually all post-eruption processes lead to increases in Fe^{3+} and derived oxygen fugacities. In Fig. 11B we plot LOI values (reflecting post-eruptive hydration/alteration) versus)NNO for

the 16 Mount Cameroon samples from this study. Symbols distinguish rapidly quenched scoria samples from more slowly cooled lava samples. The rapid quenching of scoria is apparently less important than the enhanced surface area it presents to syn- and post-eruptive fluids, because the 5 scoria samples show considerably higher values of both LOI and)NNO compared to some of the lava samples. The 3 samples with the lowest estimated)NNO values (+0.2 to +0.3) are lavas from the 1959, 1982, and 1999 eruptions (Fig. 11B).

The other method we used to estimate magmatic oxygen fugacity is based on the percentage of oxidized sulfur (S^{6+}) as opposed to reduced sulfur (S^{2-}) in glass inclusions expressed as $\%S^{6+}$, (Table 6). Although some low outliers exist, particularly in 1954 glasses, the majority of the glass inclusions yielded $\%S^{6+}$ values of 20-50, with a mean and 1Φ of 31 ∀ 15. According to the relationship between SO_4^{2+}/S^{2-} and fO_2 established by Matthews et al. (1999), these correspond to)NNO values of 0.2-1.0. Thus, these two fundamentally different techniques for estimation of oxygen fugacity are consistent, and indicate relatively high oxygen fugacities for Mount Cameroon magmas greater than the NNO buffer. Similarly high oxygen fugacities were estimated by the S-valence method for a wide range of mafic alkaline magmas by Métrich and Clocchiatti (1996).

The measured H_2O and CO_2 contents in Mount Cameroon glass inclusions (Table 7) were used to calculate saturation pressures for this mixed-volatile system using the VolatileCalc1.1 routine of Newman and Lowenstern (2002). At assumed temperatures of 1,150^oC and SiO_2 value of 46.53 wt%, the calculated pressures are 930-960 bars,

equivalent to ~3.4 km depth (assuming an upper crustal density of 2.8 g/cm^3).

Estimates for equilibration temperature and pressure for spinel-harzburgite xenolith SI2000/4 of 1,019^{o}C and 13.3 kbar were based on mineral core compositions listed in Table 4 and the T_{BKN} algorithm of Brey and Köhler (1990) and the P_{KB} algorithm of Köhler and Brey (1990), respectively. These conditions are consistent with the stability of spinel in peridotites (Herzberg, 1978; O'Neill, 1981).

Insights into Magmatic Processes from Bulk-Rock Compositions

Bulk-rock scoria and lava compositions show evidence of minor but systematic compositional differences among magmas of different historical eruptions at Mount Cameroon (Fig. 5). This minor diversity suggests different magma batches, because it can not be explained by different degrees of fractionation from a common parent magma, as seen in the Nb/Ta and Nb/Zr variations of Fig. 6. Mount Cameroon eruptions appear to be fed by ascent of small batches of magma derived from slight variations on a parental basanite melt. The typical intraplate-type characteristics of the multi-element and REE patterns for all Mount Cameroon bulk-rock samples indicate that partial melting was likely in the garnet-peridotite stability field. The ascending magmas underwent different thermal ascent paths and degrees of fractionation trends during ascent, with bulk-rock compositions from the 1982 eruption being the most primitive, and some bulk-rock compositions from the 1999 eruption the most differentiated.

Insights into Magmatic Processes from Glass-Inclusion Compositions

The glass inclusions from Mount Cameroon show considerably greater compositional variability than do their host bulk-rock samples (Fig. 8). Interestingly, this difference essentially vanishes when the full range of Mount Cameroon bulk-rock compositions is evaluated, as in Fig. 3. One possible explanation is that the trapped melts for individual eruptions may be somehow micro-sampling the broader liquid differentiation trends at play in the larger magmatic system.

The 1954 glass inclusions show a wide range in SiO_2 and include the most silica-rich glass analyzed (54-1D: 51.3 wt.%). The trends for 1954 glass inclusions, particularly the declines of CaO (Fig. 8B) and SO_3^{total} (Fig. 9A) with increased SiO_2, are consistent with simultaneous fractionation of clinopyroxene (and olivine) and degassing during ascent-related differentiation. Indeed major and volatile elements data show that the 1954 glasses also have a wide range in K_2O, CaO and S content (Fig. 9). The very silicic and K_2O-rich 1954 inclusions represent highly evolved magma. Incidentally, these same SiO_2-rich glasses have the lowest S values due to protracted and significant S degassing prior to eruption. Progressive volatile loss implies lower buoyancy and a convective process has to be visualized to explain how this fractionated, volatile-poor magma represented by these inclusions, eventually erupted in 1954. The 1954 eruption was confined to the summit crater of Mount Cameroon and produced ejecta without lava. It is envisaged that the introduction of a fresh batch of volatile-rich magma into the chamber might have triggered this eruption. By inference, melt inclusions from this fresh batch of magma should have higher MgO, CaO and S contents but lower SiO_2 content than melt inclusions of the residual, evolved, SiO_2-rich melt. The 1954 glass inclusions

have these characteristics and this magma mixing explains the wide scatter in the 1954 glass inclusion compositions from more primitive to evolved end members. Complex convective circulation processes going on in the plumbing system of basaltic volcanoes commonly mix together volatile-rich magmas with degassed magma (e.g. Stevenson and Blake, 1998; Wallace and Anderson, 1998; Sparks, 2003) and the 1954 melt inclusions attest to these processes.

The 1959 glass inclusions have the highest sulphur concentrations and most of these inclusions have sulphide grains that are spherical in shape suggesting that they were immiscible sulphide melts that quenched to these globules. The simplest explanation is that the 1959 melts were sulfide saturated upon eruption. Sulphide crystals in glass inclusions may also reflect an increase in the oxidation state of the melt through hydrogen loss from the inclusion by diffusion through the host olivine (Norman et al. 2004). In either case, the 1959 melts must have been close to sulfide saturation upon eruption.

Chlorine concentrations can also provide important insights into magmatic processes. The Mount Cameroon glass inclusions show good correlation between Cl and P, which behaves, like K, as an incompatible element in the Mount Cameroon magmatic system (Fig. 9D). This indicates a lack of significant Cl degassing.

Comparisons of Glass-Inclusion Volatile Contents Across Tectonic Settings

In Fig. 12 we show the Mount Cameroon glass inclusions from this study on H_2O variation diagrams plotted against F, CO_2, S, and Cl in comparison to a large set of glass inclusions and pillow basalt glass rims from mafic volcanic rocks in different tectonic

settings: other intraplate-type volcanoes (n = 169), mid-ocean ridge basalts (MORBs: n = 13), and subduction-related volcanoes (n = 120). The most notable feature of the Mount Cameroon glass compositions is their unusually high F contents, which are higher than any other glasses shown. Etna glass inclusions also show high F contents. Abundances of other volatile elements in Mount Cameroon glasses are generally within the broad range of those from other intraplate-type rocks. For S and Cl, Mount Cameroon glasses are intermediate between the higher values for Etna inclusions and the lower values for those from Hawaii and Piton de la Fournaise.

Conclusions

In this contribution we have provided the first data on volatile contents of trapped glass inclusions in Mount Cameroon magmas, the first estimates of magmatic temperature and oxygen fugacity, and the first data for a peridotite xenolith from this volcano, which is likely the youngest known peridotite on Earth. Bulk compositions of Mount Cameroon's intraplate-type, *nepheline*-normative basanites are very similar among the 5 eruptions investigated (1954-2000), but slight variations in the incompatible trace elements and volatiles relationships indicate the existence of differences in ascent, degassing, and differentiation histories of small magma batches. Subtle, albeit significant variations in the composition of the ejecta, lavas and glass inclusions suggest that the magmas feeding the various eruptions are not derived from a single closed magma reservoir. Sulphide globules are present as a soild phase in the 1959 glasses with the

highest S content implying that these inclusions must have been saturated in S. The most silicic 1954 inclusions have the lowest S concentration and these inclusions provide evidence of decompressive S degassing during magma ascent. The large variation in volatile content and SiO_2 concentrations for glasses of a single eruption, especially the 1954 eruption, underscores the role of mixing processes in the evolution of these magmas.

Mount Cameroon basanites have eruption temperatures of 1,150-1,200^oC and have relatively high oxygen fugacities just above the trend of the synthetic Ni-NiO buffer; this is in the realm of high oxidation exhibited by subduction-related magmatic systems. The most volatile-rich glass inclusions are the most primitive with regard to low SiO_2 (<44 wt.%) and high CaO (>12 wt.%). The one analyzed by multiple techniques has 1.7 wt% H_2O, 967 ppm CO_2, 1,530 ppm F, 2,400 ppm S, and 1,270 ppm Cl. The Mount Cameroon F contents are the highest known for basaltic glasses.

The relatively high CO_2 contents in Mount Cameroon glass inclusions supports the interpretation that the CO_2 gas responsible for the Lakes Monoun and Nyos gas disasters is magmatic in origin. The CO_2 content of the Mount Cameroon melt inclusions indicate moderate pressure of melt entrapment (~30 – 960 bars) and shallow depths of magma storage (~3.4 km). Carbon dioxide supply to Lakes Monoun and Nyos could be related to CO_2 degassing at greater depths although studies on possible depths of magma degassing at these lakes have not been done.

Acknowledgements

This study was conducted while C.E.S. fulfilled a post-doctoral fellowship in the Department of Mineral Sciences, National Museum of Natural History, Smithsonian Institution (SI), Washington D.C. under the supervision of Jim Luhr. Jim contributed significantly to this paper before his untimely death a week to when the paper was due to be submitted. The authors express appreciation to the SI for financing all laboratory work including ICP-MS analysis of bulk-rock compositions at Washington State University. The fieldwork was carried out within the framework of the British Council-funded Higher Education Link Project ("Understanding the Environment of Mount Cameroon") between the University of Buea and the University of Bristol. We are grateful for comments by R.S.J. Sparks on an earlier version of the manuscript. The revision of the final text benefited enormously from the constructive reviewer comments and criticisms provided by Anna Gioncada and Nicole Metrich as well as the editorial comments of Margaret Mangan. We acknowledge with thanks their contributions to improving this work.

References

Aka, F.T., Nagao, K., Kusakabe, M., Sumino, H., Tanyileke, G., Ateba, B., Hell, H., 2004. Symmetrical Helium isotope distribution on the Cameroon Volcanic Line, West Africa. Chemical Geology, 203, 205-223.

Anderson, A.T., and G.G. Brown, CO_2 and formation pressures of some Kilauean melt inclusions, *Am. Mineral., 78*, 794-803, 1993.

Blundy, J., Cashman, K., and Humphreys, M. (2006) Magma heating by decompression-driven crystallization beneath andesite volcanoes. Nature 443: 76-80.

Brey, G.P. & Köhler, T., 1990. Geothermometry in four-phase lherzolites II. New thermobarometers and practical assessment of existing thermobarometers. Journal of Petrology 31, 1353-1378.

Bureau, H., F. Pineau, N. Métrich, M. Semet, and M. Javoy, A melt and fluid inclusion study of the gas phase at Piton de la Fournaise volcano (Réunion Island), *Chem. Geol., 147*, 115-130, 1998.

Byers, C.D., M.O. Garcia, and D.W. Muenow, Volatiles in basaltic glasses from the East Pacific Rise at 21°N: implications for MORB sources and submarine lava flow morphology, *Earth Planet. Sci. Lett., 79*, 9-20, 1986.

Carroll, M.R., Rutherford, M.J., 1988. Sulfur speciation in hydrous experimental glasses of varying oxidation states: Results from measured wavelength shifts of sulfur X-rays. Am. Min. 73, 845-849.

Carroll, M.R. and Webser, J.D (1994) Solubilities of sulfur, noble gases, nitrogen, chlorine, and fluorine in magmas. In: Carroll, M.R. and Holloway, J.R., eds, Volatiles in Magmas, Reviews in Mineralogy 30, Mineralogical Society of America: 231-271.

Cervantes P, Wallace P (2003) Magma degassing and basaltic eruption styles: A case study of ~2000 yr BP Xitle volcano in central Mexico. Journal of Volcanology and Geothermal Research 120: 249-270.

Danyushevsky, L.V., Falloon, T.J., Sobolev, A.V., Crawford, A.J., Carroll, M., Price, R.C. 1993. The H_2O content of basalt glasses from Southwest Pacific back-arc basins. Earth and Planetary Science Letters 177, 347-362.

Danyushevsky, L.V., McNeill, A.W., Sobolev, A.V. 2002. Experimental and petrological studies of melt inclusions in phenocrysts from mantle-derived magmas: an overview of techniques, advantages and complications. Chemical Geology 183, 5-24.

Davis, M.G., Garcia, M.O., Wallace, P., 2003. Volatiles in glasses from Mauna Loa

volcano, Hawaii: implications for mantle degassing and contamination, and growth of Hawaiian volcanoes. Contributions to Mineralogy and Petrology 144, 570-591.

Déruelle, B., N'ni, J., Kambou, R., 1987. Mount Cameroon: an active volcano of the Cameroon Line. Journal of African Earth Sciences 6, 197-214.

Dixon, J.E., D.A. Clague, and E.M. Stolper, 1991 Degassing history of water, sulfur, and carbon in submarine lavas from Kilauea volcano, Hawaii, J. Geol., 99, 371-394.

Dixon, JE, Clague DA (2001) Volatiles in basaltic glasses from Loihi Seamount, Hawaii: Evidence for a relatively dry plume component. Journal of Petrology 42: 627-654.

Fitton, J.G., and Dunlop, H., 1985. The Cameroon Line, West Africa, and its bearing on the origin of oceanic and continental alkali basalt. Earth and Planetary Science Letters 72: 23-38.

Fitton, J.G., Kilburn, C.R.J., Thirlwall, M.F., Hughes, D.J., 1983. 1982 eruption of Mount Cameroon, West Africa. Nature 306, 327-332.

Geze, B., 1953. Les volcans du Cameroun occidental. Bulletin of Volcanology 13, 63-92.

Gioncada, A., Clocchiatti, R., Sbrana, A., Bottazzi, P., Massare, D. and Ottolini, L.

(1998): A study of melt inclusions at Vulcano (Aeolian Islands, Italy): insights on the primitive magmas and on the volcanic feeding system. Bulletin of Volcanology, 60, 286-306.

Gurenko, A.A., Hansteen, T.H. and Schmincke, H-U (1996): Evolution of parental magmas of Miocene shield basalts of Gran Canaria (Canary Islands): constraints from crystal, melt and fluid inclusions in minerals. Contributions to Mineralogy and Petrology, 124, 422-435.

Gurenko, A.A., Belousov, A.B., Trumbull, R.B., and Sobolev, A.V. (2005) Explosive basaltic volcanism of the Chikurachki Volcano (Kurile Arc, Russia): Insights on pre-eruptive magmatic conditions and volatile budget revealed from phenocryst-hosted melt inclusions and groundmass glasses. Journal of Volcanology and Geothermal Research 147: 203-232.

Halliday, A.N., Davidson, J.P., Holden, P., DeWolf, C., Lee, D.-C., and Fitton, J.G. (1990) Trace-element fractionation in plumes and the origin of HIMU mantle beneath the Cameroon line. Nature 347: 523-528.

Harte, B., 1977. Rock nomenclature with particular relation to deformation and recrystallization textures in olivine xenoliths. Journal of Geology 85, 279-288.

Hauri, E., Wang, J., Dixon, J.E., King, P.L., Mandeville, C., Newman, S. (2002) SIMS

analysis of volatiles in silicate glasses 1. Calibration, matrix effects, and comparisons with FTIR. Chem. Geol. 183, 99-114.

Hauri, E., 2002. SIMS analysis of volatiles in silicate glasses, 2: isotopes and abundances in Hawaiian melt inclusions. Chemical Geology 183, 115-141.

Herzberg, C.T., 1978. Pyroxene geothermometry and geobarometry: Experimental and thermodynamic evaluation of some subsolidus phase relations involving pyroxenes in the system CaO-MgO-Al2O3-SiO2. Geochimica et Cosmochimica Acta 42, 945-957.

Huebner, J.S., Sato, M., 1970. The oxygen fugacity-temperature relationships of manganese oxide and nickel oxide buffers. Am. Mineral. 55, 934-952.

Jarosewich, E., Nelen, J.A., Norberg, J.A., 1980. Reference samples for electron microprobe analysis. Geostand. Newslett. 4, 43-47.

Jugo, P.J., Luth, R.W., Richards, J.P., 2005. Experimental data on the speciation of sulfur as a function of oxygen fugacity in basaltic melts. Geochim. Cosmochim. Acta 69, 497-503.

Keppler, H., 1999. Experimental evidence for the source of excess sulfur in explosive volcanic eruptions. Science 284, 1652-1654.

Köhler, T.P. & Brey, G.P., 1990. Calcium exchange between olivine and clinopyroxene calibrated as a geothermobarometer for natural peridotites from 2 to 60 kb with applications. Geochimica et Cosmochimica Acta 54, 2375-2388.

Kress, V.C., Carmichael, I.S.E., 1991. The compressibility of silicate liquids containing Fe_2O_3 and the effect of composition, temperature, oxygen fugacity and pressure on their redox states. Contributions to Mineralogy and Petrology 108, 82-92.

Le Bas, M. J., Le Maitre, R. W., Streckeisen, A., and Zanettin, B., 1986, A chemical classification of volcanic rocks based on the total alkali-silica diagram: Journal of Petrology, v. 27, p. 745-750.

Le Guern, F., Sigvaldason, G.E. (Editors) 1989. The lake Nyos event and natural CO_2 degassing, I. Journal of Volcanology and Geothermal Research 39, Special Issue.

Loucks, R.R., 1996. A precise olivine-augite Mg-Fe-exchange geothermometer. Contributions to Mineralogy and Petrology 125, 140-150.

Luhr, J.F., 2001. Glass inclusions and melt volatile contents at Parícutin Volcano, Mexico. Contributions to Mineralogy and Petrology 142, 261-283.

Luhr, J.F., Aranda-Gómez, J.J., and Pier, J.G. (1989) Spinel-lherzolite-bearing Quaternary volcanic centers in San Luis Potosi, México: I. Geology, mineralogy, and petrology. J Geophys Res 94, B6: 7916-7940.

Luhr, J.F., and Haldar, D. (2006) Barren Island Volcano (NE Indian Ocean): Island-arc high-alumina basalts produced by troctolite contamination. Journal of Volcanology and Geothermal Research, 149: 177-212.

Marzoli, A., Renne, P.R., Piccirillo, E.M., Francesca, C., Bellieni, G., Melfi, A.J., Nyobe, J.B., N'ni, J., 1999. Silicic magmas from the continental Cameroon Volcanic Line (Oku, Bambouto and Ngaoundere): $^{40}Ar/^{39}Ar$ dates, petrology, Sr-Nd-O isotopes and their petrogenetic significance. Contributions to Mineralogy and Petrology 135, 133-150.

Matthews, S.J., Moncrieff, D.H.S., Carroll, M.R., 1999. Empirical calibration of the sulphur valence oxygen barometer from natural and experimental glasses: Methods and applications. Min. Mag. 63, 3, 421-431.

Melson, W.G., 1983. Monitoring the 1980-1982 eruptions of Mount St. Helens: compositions and abundances of glass. Science 221, 1387-1391.

Métrich, N., Allard, P., Spilliaert, N., Andronico, D., Burton, M. (2004) 2001 flank eruption of the alkali- and volatile-rich primitive basalt responsible for Mount Etna's

evolution in the last three decades. Earth and Planetary Science Letters 228: 1-17.

Métrich, N., Bertagnini, A., Landi, P, Rosi, M. (2001) Crystallization driven by decompression and water loss at Stromboli Volcano (Aeolian Islands, Italy). Journal of Petrology 42: 1471-1490.

Métrich, N., Clocchiatti, R., 1996. Sulfur abundance and its speciation in oxidized alkaline melts. Geochim. Cosmochim. Acta 60, 21, 4151-4160.

Métrich, N., R. Clocchiatti, M. Mosbah, and M. Chaussidon, The 1989-1990 activity of Etna: magma mingling and ascent of H_2O-Cl-S rich basaltic magma. Evidence from melt inclusions. J. Volcanol. Geotherm. Res., 59, 131-144, 1993.

Naumov, V.B., Kovalenko, V.I., Dorofeeva, V.A., and Yarmolyuk, V.V. (2004) Average concentrations of major, volatile, and trace elements in magmas of various geodynamic settings. Geochemistry International 42: 977-987.

Newman, S. and Lowenstern, J.B. (2002) VolatileCalc: a silicate melt-H_2O-CO_2 solution model written in Visual Basic for excel. Computers and Geosciences 28: 597-604.

Ngounouno, I., Deruelle, B., Montigny, R., Demaiffe, D. 2004. Petrology and geochemistry of monchiquites from Tchircotche (Garoua rift, north Cameroon, Central

Africa). Mineralogy and Petrology DOI 10.1007/s00710-004-0068-y.

Nilsson, K., Peach, C.L., 1993. Sulfur speciation, oxidation state, and sulfur concentration in backarc magmas. Geochim. Cosmochim. Acta 57, 3807-3813.

Norman, M.D., Garcia, M.O., Bennett, V.C. 2004. Rhenium and chalcophile elements in basaltic glasses from Ko'olau and Moloka'i volcanoes: magmatic outgassing and composition of the Hawaiian plume. Geochimica et Cosmochimica Acta 68, 3761-3777.

Norman, M.D., Garcia, M.O., Kamenetsky, V.S., Nielsen, R.L., 2002. Olivine-hosted melt inclusions in Hawaiian picrites: equilibration, melting, and plume source characteristics. Chemical Geology 183, 143-168.

O'Neill, H.S.C., 1981. The transition between spinel lherzolite and garnet lherzolite, and its use as a geobarometer. Contributions to Mineralogy and Petrology 77, 185-194.

Peck, L.C. (1964) Systematic analysis of silicates. U.S. Geol. Surv. Bull. 1170, 89.

Princivalle, F., Salviulo, G., Marzoli, A., Piccirillo, E.M., 2000. Clinopyroxene of spinel-peridotite mantle xenoliths from Lake Nji (Cameroon volcanic line, West Africa): crystal chemistry and petrological implications. Contributions to Mineralogy and Petrology 139, 503-508.

Rankenburg, K., Lassiter, J.C. and Brey, G., 2004a. Origin of megacrysts in volcanic rocks of the Cameroon volcanic chain – constraints on magma genesis and crustal contamination. Contributions to Mineralogy and Petrology 147, 129-144.

Rankenburg, K., Lassiter, J.C. and Brey, G., 2004b. The role of continental crust and lithospheric mantle in the genesis of Cameroon volcanic line lavas: constraints from isotopic variations in lavas and megacrysts from the Biu and Jos Plateaux. Journal of Petrology 46, 169-190.

Rhodes, J.M. and Vollinger, M.J. (2005) Ferric/ferrous ratios in 1984 Mauna Loa lavas: a contribution to understanding the oxidation state of Hawaiian magmas. Contributions to Mineralogy and Petrology 149: 666-674.

Roggensack K, Hervig RL, McKnight SB, Williams SN (1997) Explosive basaltic volcanism from Cerro Negro volcano: Influence of volatiles on eruptive style. Science 277:1639-1642.

Sato, H., Aramaki, S., Kusakabe, M., Hirabayashi, J.-I., Sano, Y., Nogiri, Y., and Tchoua, F. (1990) Geochemical difference of basalts between polygenetic and monogenetic volcanoes in the central part of the Cameroon volcanic line. Geochemical Journal 24: 357-370.

Saito, G., Uto, K., Kazahaya, K., Shinohara, H., Kawanabe, Y., Satoh, H. (2005) Petrological characteristics and volatile content of magma from the 2000 eruption of Miyakejima Volcano, Japan. Bulletin of Volcanology 67: 268-280.

Scaillet, B., Clemente, B., Evans, B.W., Pichavant, M., 1998. Redox control of sulfur degassing in silicic magmas. J. Geophys. Res. 103, 23937-23949.

Siebert, L., Simkin, T., 2002-. Volcanoes of the world: an illustrated catalog of Holocene volcanoes and their eruptions. Smithsonian Institution, Global Volcanism Program Digital Information Series, GVP-3, (http://www.volcano.si.edu/gvp/world/).

Sisson, T.W., and S. Bronto, Evidence for pressure-release melting beneath magmatic arcs from basalt at Galunggung, Indonesia, Nature, 391, 883-886, 1998.

Sisson, T.W., Layne, G.D., 1993. H_2O in basalt and basaltic andesite glass inclusions from four subduction-related volcanoes. Earth and Planetary Science Letters 117, 619-635.

Sours-Page, R., Nielsen, R.L., Batiza, R., 2002. Melt inclusions as indicators of parental magma diversity on the northern East Pacific Rise. Chemical Geology 183, 237-261.

Sparks, R.S.J., 2003. Dynamics of magma degassing. In: Oppenheimer, C., Pyle, D.M.,

Barclay, J. (Eds.), Volcanic degassing. Geological Society of London Publications, 213, 5-22.

Spilliaert, N., Métrich, N., and Allard, P. (2006) S-Cl-F degassing pattern of water-rich alkali basalt: Modelling and relationship with eruption styles on Mount Etna volcano. Earth and Planetary Science Letters 248: 772-786.

Stevenson, D.S. and Blake, S. 1998. Modelling the dynamics and thermodynamics of volcanic degassing. Bulletin of Volcanology, 60, 307-317.

Sugawara, T. 2000. Empirical relationships between temperature, pressure, and MgO content in olivine and pyroxene saturated liquid. Journal of Geophysical Research 105, 8457-8472.

Suh, C.E., Sparks, R.S.J., Fitton, J.G., Ayonghe, S.N., Annen, C., Nana, R., Luckman, A., 2003. The 1999 and 2000 eruptions of Mount Cameroon: eruption behaviour and petrochemistry of lava. Bulletin of Volcanology 65, 267-281.

Suh, C.E., Sparks, R.S.J., Fitton, J.G., Ayonghe, S.N., Annen, C., Nana, R., Luckman, A., 2005. The 1999 and 2000 eruptions of Mount Cameroon: eruption behaviour and petrochemistry of lava [Erratum]. Bulletin of Volcanology 67, 388-390.

Sun, S.S., McDonough, W.F., 1989. Chemical and isotopic systematics of oceanic

basalts; implications for mantle composition and processes. In: Saunders, A.D., Norry, M.J. (eds.) Magmatism in the ocean basins. Geol. Soc. Spec. Pub. 42, 313-345.

Turner S. P., Hawkesworth C. J., Rogers N. W., King P. (1997) U-Th isotope disequilibria and ocean island basalt generation in the Azores. Chem. Geol. 139:145-164.

Ulmer P (1989) The dependence of Fe^{2+}-Mg cation-partitioning between olivine and basaltic liquid on pressure, temperature, and composition: An experimental study to 30 kbars. Contrib Mineral Petrol 101:261-273

Venzke, E., Wunderman, R.W., McClelland, L., Simkin, T., Luhr, J.F., Siebert, L., Mayberry, G. (eds.), 2002-. Global volcanism, 1968 to the present. Smithsonian Institution, Global Volcanism Program Digital Information Series, GVP-4 (http://www.volcano.si.edu/gvp/reports/).

Vogel, T.A., Aines, R., 1996. Melt inclusions from chemically zoned ash flow sheets from the Southwest Nevada volcanic field. Journal of Geophysical Research 101, 5591-5610.

Wade, J.A., Plank, T., Melson, W.G., Soto, G.J., and Hauri, E.H. (2004) The volatile content of magmas from Arenal volcano, Costa Rica. Journal of Volcanology and Geothermal Research 157: 94-120.

Wallace, P.J. and Anderson, A.T., 1998. Effects of eruption and lava drainback on the H2O contents of basaltic magmas at Kilauea volcano. Bulletin of Volcanology, 59, 327-344.

Wallace, P., Carmichael, I.S.E., 1994. S speciation in submarine basaltic glasses as determined by measurements of SK X-ray wavelength shifts. American Mineralogist. 79, 161-167.

Witter, J.B., Kress, V.C., Delmelle, P., Stix, J. (2004) Volatile degassing, petrology, and magma dynamics of the Villarrica Lava Lake, Southern Chile. J. Volcanol. Geotherm. Res. 134: 303-337.

Wolff J. A., Grandy J. S., Larson P. B. (2000) Interaction of mantle-derived magma with island crust? Trace element and oxygen isotope data from the Diego Hernandez Formation, Las Cañadas, Tenerife. J. Volcanol. Geotherm. Res. 103: 343-366.

List of Tables

Table 1: Modes of Mount Cameroon tephra samples for the different eruption years. Modes determined by point counting of more than 1000 points on a single thin section in cross-polarized transmitted and reflected light. Modal data for peridotite nodule recovered from 2000 eruption tephra is also included.

Table 2: Representative major and trace element analyses of Mount Cameroon tephra and lava samples for the five eruptions studied.)NNO values are calculated after Kress and Carmichael (1991).

Table 3. Olivine-clinopyroxene pairs for tephra samples from Mount Cameroon used in calculating liquidus temperature (T, ^{o}C) based on the method of Loucks (1996).

Table 4: Mineral chemistry of main phenocryst phases in the peridotite nodule from Mount Cameroon. Mg# for spinel is based on Fe_{total} . Mg# based on cation numbers indicated. Standard deviation at 1σ.

Table 5: Petrographic characteristics of olivine-hosted glass inclusions studied by electron microprobe. For triangular prism shapes x,y,z are length, triangle base, triangle height; for the irregular shape x,y,z represent the three major dimensions; for elongated x,y,z are the three principal diameters; and for the rod shape x is the length and y the basal diameter. Devitrified glasses are not listed.

Table 6: Representative olivine-hosted melt inclusion composition (determined by EMP, see Luhr 2001 for analytical conditions) for five eruptions of Mount Cameroon. S^t is sulphur in the reduced form and S^{6+} is sulphur in the form of sulphate. Total sulphur as SO_3^t. Liquidus temperature (T, ^oC) is after Sugawara (2000).

Table 7: LA-ICP-MS analysis of melt inclusions at Mount Cameroon volcano. Analytical precision given in % is calculated as 1/background-corrected counts)1/2.

Table 8: Ion probe data for volatile elements in melt inclusions at Mount Cameroon.

Table 9: FTIR-measured H_2O (wt%) and CO_2 (ppm) content of representative melt inclusions at Mount Cameroon volcano. Sample numbers same as in Table 3.

List of Figures

Fig. 1 - Volcanoes of the Cameroon Volcanic Line (CVL). Mount Cameroon lies just landward of the ocean-continent boundary.

Fig. 2 - Sketch map of the geology of Mount Cameroon Volcano with the locations of scoria and lava samples considered in this study

Fig. 3 - Total Alkalies versus Silica (TAS) classification diagram (Le Bas et al., 1986) showing bulk-rock compositions reported by Fitton et al. (1983), Déruelle et al (1987), Sato et al. (1990), Suh et al. (2005), and this study (Table 2).

Fig. 4 - (A) Multi-element plot normalized to the primitive mantle composition of Sun and McDonough (1989). Two Mount Cameroon samples are shown, which represent the lowest (SI82/3) and highest (SI99/3) values for most of these elements in the analyzed suite. Also shown are a basanite from the Diego Hernandez Formation, Las Cañadas, Tenerife, Canary Islands (DH97-18B: Wolff et al., 2000), a basanite from the 1652 eruption of São Miguel island in the Azores (S7: Turner et al., 1997), and a spinel-lherzolite-bearing basanite from the Ventura volcanic field of central Mexico (SLP-34: Luhr et al., 1989). (B) REE plot normalized to the chondrite composition of Sun and McDonough (1989), with samples as in A.

Fig. 5 - SiO_2 variation diagrams for the 5 scoria and 11 lava samples from Table 2. (A)

CaO, (B) Sc, (C) Co, (D) K_2O, (E) Sr, and (F) Ta. Major elements are normalized to 100% without LOI and with Fe^{3+} = 15% Fe^{total}. Trace element binary plots for Sc-Nb (G) and Co-Nb show negative correlations while the trend for the incompatible elements Ba (I), Rb (J) and Zr (K) against Nb show positive trends. Correlation coefficients (R^2) are listed on each plot.

Fig. 6 - (A) Th versus Nb/Ta, and (B) MgO vs Nb/Zr for the 5 scoria and 11 lava samples from Table 2.

Fig. 7 - Backscattered-electron images showing petrographic characteristics (shapes, sizes, inclusions) of four representative studied glass inclusions from Mount Cameroon volcano. (A) spherical glass inclusion with a subhedral spinel (white) crystal: sample SI2000-5E2; (B) elongated glass inclusion with exposed bubble; three light-colored spots show locations of electron-microprobe analyses with a 10-:n diameter beam: sample SI99-1A; (C) elongated, lensoid glass inclusion: sample SI2000-5E3, (D) several glass inclusions hosted by a single olivine crystal. The largest inclusion (SI82-3C1) is irregular in shape and has an exposed spherical bubble whereas the smaller glass inclusions are more spherical in shape. These inclusions are compositionally identical.

Fig. 8 - SiO_2-variation diagrams showing both bulk-rock (solid symbols) and glass inclusion (open symbols) compositions: (A) K_2O, (B) CaO, (C) electron-microprobe totals, which provide an estimate of the glass H_2O contents by difference (100% minus

EMP total), and (D) host-olivine Mg#.

Fig. 9 - Variations of SO_3^{total} and Cl in glass inclusions versus SiO_2 and P_2O_5; the latter behaves incompatibly in the Mount Cameroon magmas. SiO_2 versus (A) SO_3^{total} and (C) Cl; P_2O_5 versus (B) SO_3^{total} (D) Cl and (E) K_2O. On panel A, the four glass inclusions analyzed by FTIR, SIMS, and LA-ICP-MS are labeled. (F): Variation of Na2O/TiO2 versus CaO/Al2O3, ratios that are unrelated to post-entrapment compositional modifications of melt inclusions.

Fig. 10 - (A) Multi-element plot normalized to the primitive mantle composition of Sun and McDonough (1989). The same two Mount Cameroon bulk-rock samples from Fig. 4 are shown, which represent the lowest (SI82/3) and highest (SI99/3) values for nearly all of these elements in the analyzed suite. Pb is an exception since SI99/3 has anomalously low Pb. Also shown are LA-ICP-MS data for 3 Mount Cameroon glass inclusions (Table 8); the glass-inclusion Pb values are within the total range of bulk-rock samples. (B) REE plot normalized to the chondrite composition of Sun and McDonough (1989), with samples as in A.

Fig. 11 - (A) Temperature estimates for Mount Cameroon magmas by the methods of Sugawara (2000) and Loucks (1996) plotted against eruption year. (B) Relative oxygen fugacity expressed as)NNO (Table 2) plotted against loss on ignition (LOI) values, also from Table 2. The three labeled samples with lowest)NNO are thought to provide the

best estimate for oxygen fugacity in Mount Cameroon basanites.

Fig. 12 - Comparison of volatiles in Mount Cameroon glass inclusions with those from glass inclusions and pillow basalt glasses from different tectonic environments. (A) H_2O versus F, (B) H_2O versus CO_2, (C) H_2O versus S, and (D) H_2O versus Cl. Sources of data: Mount Cameroon (Table 6); Hawaii (Dixon et al., 1991; Anderson and Brown, 1993; Davis et al., 2003); Piton de la Fournaise (Bureau et al., 1998); Etna (Métrich et al., 1993; Métrich et al., 2004; Spilliaert et al., 2006); MORB (Byers et al., 1986); various subduction-zone volcanoes (Sisson and Layne, 1993; Roggensack et al., 1997; Sisson and Bronto, 1998; Luhr, 2001; Métrich et al., 2001; Saito et al., 2001; Cervantes and Wallace, 2003; Witter et al., 2004; Gurenko et al., 2005; and Wade et al., 2006). Also shown as three stars are geometric mean values for glasses from 3 tectonic settings (M = MORBs, OIB = ocean island basalts, and SZ = subduction zones: labeled on panel A) from a large compilation (Naumov et al., 2004).

Table 1. Point-counted modes.

Eruption year:	1954	1959	1982	1999	2000	1959
Sample type:	Scoria	Scoria	Scoria	Scoria	Scoria	Lava
Sample number:	SI54/1	SI59/1	SI82/3	SI99/4	SI2000/5	SI59/2
Latitude:	4°20'50"N	4°15'40"N	4°09'42"N	4°09'17"N	4°12'29"N	4°15'40"N
Longitude:	9°17'38"E	9°15'37"E	9°07'35"E	9°08'17"E	9°10'21"E	9°15'37"E
Elevation (m):	4,000	1,833	2,744	2,746	3,807	1,732
Point counting (vol%, vesicles free)						
Olivine phen.	7.7	0.3	1.1	2.9	1.3	2.5
Olivine microphen.	1.4	1.0	3.0	1.1	0.3	3.1
Cpx phen.	4.9	6.9	1.9	7.3	8.8	3.0
Cpx microphen.	12.1	9.3	3.6	3.4	3.7	2.5
Fe-Ti Ox. microphen.	3.2	3.9	0.0	0.9	1.6	1.1
Plag. phen.	4.1	6.9	0.0	3.0	2.5	5.3
Plag. microphen.	12.2	15.2	0.0	7.0	5.0	16.2
Opx (xenolith)						
Spinel (xenolith)						
Groundmass	54.4	56.5	90.4	74.4	76.8	66.3

Mineral abbreviations: Cpx = clinopyroxene, Fe-Ti Ox. = Fe-Ti oxides, Plag = plagioclase, Opx = orthopyroxene.
Phenocrysts (phen) >0.3 mm; microphenocrysts (microphen.) <0.3 mm & >0.03 mm; Groundmass <0.03 mm.
Maximum grain sizes in xenolith SI2000/4: olivine and opx = 0.5 mm, cpx = 1.8 mm, and spinel = 1.5 mm.

Table 1. Continued

Eruption year:	1959	1959	1982	1982	1999	1999
Sample type:	Lava	Lava	Lava	Lava	Lava	Lava
Sample number:	SI59/3	SI59/4	SI82/1	SI82/2	SI99/1	SI99/2
Latitude:	4°15'33"N	4°15'19"N	4°08'23"N	4°09'42"N	4°06'11"N	4°07'53"N
Longitude:	9°15'46"E	9°15'57"E	9°06'27"E	9°07'35"E	9°07'04"E	9°07'44"E
Elevation (m):	1,700	1,517	1,958	2,744	1,545	2,090
Point counting (vol%, vesicles free)						
Olivine phen.	2.3	3.3	0.1	0.3	6.1	3.7
Olivine microphen.	2.8	1.5	0.4	1.4	1.7	3.1
Cpx phen.	4.1	3.7	0.1	0.0	2.4	2.1
Cpx microphen.	3.2	2.2	0.6	0.8	3.3	4.2
Fe-Ti Ox. microphen.	0.9	1.3	0.0	0.1	1.1	0.5
Plag. phen.	2.4	2.2	0.0	0.0	2.3	1.1
Plag. microphen.	6.5	4.7	0.8	1.2	2.5	0.8
Opx (xenolith)						
Spinel (xenolith)						
Groundmass	77.8	81.1	98.0	96.2	80.6	84.5

Table 1. Continued

Eruption year:	1999	2000	2000	2000	2000
Sample type:	Lava	Lava	Lava	Lava	Xenolith
Sample number:	SI99/3	SI2000/1	SI2000/2	SI2000/3	SI2004/4
Latitude:	4°09'18"N	4°12'40"N	4°12'40"N	4°12'38"N	4°12'28"N
Longitude:	9°08'17"E	9°10'37"E	9°10'37"E	9°10'37"E	9°10'21"E
Elevation (m):	2,734	3,880	3,880	3,730	3,807
Point counting (vol%, vesicles free)					
Olivine phen.	4.1	3.1	3.3	4.2	74.4
Olivine microphen.	3.5	2.2	4.6	1.9	
Cpx phen.	2.7	6.4	5.3	6.3	3.9
Cpx microphen.	6.2	3.7	3.1	2.4	
Fe-Ti Ox. microphen.	2.0	0.9	1.0	1.8	
Plag. phen.	2.7	0.3	0.8	1.1	
Plag. microphen.	3.1	1.5	1.4	1.8	
Opx (xenolith)					20.6
Spinel (xenolith)					1.1
Groundmass	75.7	81.9	80.5	80.5	

Table 2. Bulk-rock compositions of Mount Cameroon scoria and lava samples

Year:	1954	1959	1982	1999	2000	1959	1959	1959
Type:	Scoria	Scoria	Scoria	Scoria	Scoria	Lava	Lava	Lava
Sample	SI54/1	SI59/1	SI82/3	SI99/4	SI2000/5	SI59/2	SI59/3	SI59/4
XRF (wt.%)								
SiO_2	45.63	46.33	44.41	46.15	45.71	46.58	46.13	46.49
TiO_2	3.12	3.25	3.50	3.20	3.10	3.24	3.32	3.34
Al_2O_3	15.01	15.97	15.28	15.45	14.81	16.31	16.46	16.18
Fe_2O_3	4.29	3.41	5.24	4.29	3.98	2.96	2.90	3.34
FeO	7.57	7.67	7.60	7.30	7.80	8.00	8.33	7.94
MnO	0.20	0.20	0.20	0.20	0.20	0.20	0.20	0.20
MgO	7.21	5.86	6.19	6.61	7.37	5.44	5.29	5.47
CaO	11.01	10.39	11.89	10.47	11.03	9.97	10.25	10.29
Na_2O	3.77	4.18	3.46	3.89	3.77	4.45	4.33	4.32
K_2O	1.45	1.74	1.28	1.59	1.49	1.84	1.78	1.81
P_2O_5	0.65	0.80	0.55	0.69	0.65	0.84	0.82	0.82
LOI	-0.34	-0.33	-0.30	-0.31	-0.43	-0.43	-0.41	-0.39
Total	99.57	99.47	99.30	99.53	99.48	99.40	99.40	99.81
CIPW norm (wt.%)								
or	8.57	10.34	7.62	9.46	8.81	10.93	10.58	10.70
ab	13.88	16.86	11.10	16.55	13.60	17.94	16.76	17.07
an	19.84	19.72	22.52	20.04	19.15	19.16	20.28	19.38
ne	9.81	10.12	9.98	8.96	9.96	10.72	10.81	10.56
di	25.06	21.92	27.35	22.53	25.65	20.46	20.82	21.58
ol	12.61	10.40	10.45	12.06	12.66	10.08	9.88	9.85
mt	2.77	2.61	3.00	2.71	2.75	2.58	2.65	2.64
il	5.94	6.19	6.70	6.10	5.91	6.17	6.32	6.34
ap	1.51	1.85	1.27	1.60	1.51	1.95	1.90	1.90
?NNO	1.4	0.8	1.8	1.5	1.1	0.4	0.3	0.7
XRF (ppm)								
V	295	266	337	274	282	246	258	259
Cr	213	76	40	90	204	44	43	44
Co	46	37	47	42	45	35	37	36
Ni	99	59	65	80	98	48	46	52
Cu	76	59	106	68	71	62	73	72
Zn	113	113	152	123	118	117	115	111
ICP-MS (ppm)								
Sc	26.0	21.3	30.0	22.9	26.1	18.1	19.4	19.6
Rb	36.6	40.2	29.1	36.8	36.8	42.3	41.7	41.5
Sr	1077	1101	906	1045	1058	1140	1150	1145
Y	33.35	35.96	31.02	33.87	32.99	36.83	36.21	36.17
Zr	339	373	288	347	338	386	379	378
Nb	96.2	105.6	75.6	98.1	95.9	111.0	109.7	109.1
Cs	0.42	0.49	0.34	0.42	0.43	0.51	0.48	0.49
Ba	450	516	371	466	452	537	528	521
La	73.8	83.1	59.5	74.4	73.6	86.7	85.0	84.7
Ce	137.1	157.0	113.7	139.9	137.2	163.3	160.2	159.3
Pr	15.19	17.43	12.89	15.53	15.18	18.16	17.69	17.61
Nd	59.2	68.2	51.6	60.4	59.1	70.3	68.8	68.5
Sm	11.57	13.58	10.73	11.84	11.56	13.78	13.48	13.53
Eu	3.56	4.10	3.34	3.67	3.58	4.18	4.08	4.01
Gd	9.38	10.89	9.13	9.77	9.43	11.15	10.87	10.83
Tb	1.29	1.52	1.29	1.37	1.33	1.54	1.53	1.51
Dy	6.98	8.01	6.77	7.27	6.95	8.11	8.03	7.93
Ho	1.25	1.45	1.21	1.30	1.25	1.48	1.44	1.42
Er	3.02	3.44	2.93	3.14	3.01	3.51	3.39	3.44
Tm	0.40	0.45	0.38	0.41	0.39	0.46	0.45	0.45
Yb	2.26	2.53	2.12	2.36	2.26	2.61	2.61	2.58
Lu	0.33	0.38	0.31	0.35	0.33	0.39	0.38	0.38
Hf	7.63	8.45	6.93	7.72	7.57	8.48	8.38	8.41
Ta	5.98	6.76	4.80	6.11	5.94	7.06	6.96	6.93
Pb	3.51	4.68	2.88	3.29	3.62	3.50	3.94	3.84
Th	8.14	8.79	6.22	8.16	8.13	9.30	9.16	9.16
U	1.99	2.18	1.51	2.01	1.97	2.30	2.30	2.27

CIPW norms assume Fe^{3+} = 15% of Fe^{total} and were calculated for major elements normalized to 100% without LOI.

Table 2. Continued

Year:	1982	1982	1999	1999	1999	2000	2000	2000
Type:	Lava	Lava	Lava	Lava	Lava	Lava	Lava	Lava
Sample	SI82/1	SI82/2	SI99/1	SI99/2	SI99/3	SI2000/1	SI2000/2	SI2000/3
XRF (wt.%)								
SiO_2	45.38	44.71	46.47	47.59	47.69	45.99	46.06	45.99
TiO_2	3.51	3.50	3.21	3.07	3.07	3.15	3.17	3.14
Al_2O_3	15.83	15.21	15.78	17.00	17.16	15.17	15.18	15.03
Fe_2O_3	3.04	4.51	2.88	3.25	3.30	3.38	3.33	3.97
FeO	9.53	8.33	8.69	7.09	6.98	8.45	8.60	7.88
MnO	0.20	0.20	0.20	0.20	0.20	0.20	0.20	0.20
MgO	5.84	6.24	6.29	4.82	4.57	7.08	6.90	6.92
CaO	11.48	12.03	10.58	9.42	9.26	11.03	10.90	11.18
Na_2O	3.63	3.51	4.02	4.75	4.83	3.79	3.78	3.73
K_2O	1.38	1.26	1.65	1.97	2.01	1.49	1.50	1.46
P_2O_5	0.66	0.54	0.73	0.87	0.87	0.67	0.70	0.66
LOI	-0.65	-0.39	-0.58	-0.28	-0.32	-0.44	-0.53	-0.49
Total	99.83	99.65	99.92	99.75	99.62	99.96	99.79	99.67
CIPW norm (wt.%)								
or	10.58	7.45	10.64	11.64	11.88	8.81	10.64	10.64
ab	15.91	11.14	16.85	21.19	21.81	14.29	16.47	16.66
an	19.14	22.06	19.37	19.26	19.27	19.92	19.28	19.29
ne	10.91	10.10	10.59	10.34	10.37	9.59	10.75	10.69
di	21.38	28.07	21.46	17.94	17.34	24.71	21.49	21.46
ol	11.04	10.26	10.18	9.36	9.06	12.40	10.43	10.32
mt	2.93	3.00	2.71	2.42	2.41	2.77	2.78	2.75
il	6.25	6.67	6.32	5.83	5.85	5.96	6.31	6.31
ap	1.88	1.25	1.90	2.02	2.02	1.55	1.88	1.90
?NNO	0.2	1.3	0.2	0.9	0.9	0.6	0.6	1.1
XRF (ppm)								
V	312	331	266	220	224	272	275	279
Cr		37	106	14	9	151	158	178
Co	43	46	38	31	29	43	42	39
Ni	58	65	74	33	32	88	92	89
Cu	111	105	85	54	52	81	80	86
Zn	136	111	134	108	106	152	134	131
ICP-MS (ppm)								
Sc	25.1	30.8	22.3	16.1	14.8	25.1	24.4	25.8
Rb	32.9	28.7	38.0	46.8	46.7	37.0	36.4	36.2
Sr	1021	917	1055	1196	1227	1063	1041	1046
Y	32.93	31.14	33.99	37.59	37.93	33.31	32.54	32.93
Zr	318	288	348	404	410	340	333	334
Nb	87.0	75.5	98.6	119.8	122.3	96.8	94.9	94.6
Cs	0.4	0.34	0.45	0.54	0.54	0.43	0.43	0.41
Ba	425	370	473	567	581	456	446	446
La	68.7	59.4	76.2	90.8	92.7	74.4	73.2	72.6
Ce	130.4	113.5	143.3	168.4	172.2	139.1	136.4	136.4
Pr	14.62	12.90	15.90	18.43	18.73	15.37	15.08	15.11
Nd	58.1	51.5	61.9	70.6	71.7	59.6	58.4	58.5
Sm	11.73	10.78	12.28	13.49	13.63	11.75	11.41	11.57
Eu	3.64	3.34	3.72	4.10	4.11	3.59	3.48	3.55
Gd	9.81	9.24	9.95	10.92	10.88	9.64	9.50	9.41
Tb	1.37	1.27	1.39	1.51	1.51	1.34	1.30	1.31
Dy	7.32	6.85	7.37	8.06	8.11	7.14	6.93	6.97
Ho	1.30	1.24	1.33	1.45	1.46	1.28	1.26	1.24
Er	3.11	2.93	3.18	3.44	3.53	3.06	2.98	2.99
Tm	0.40	0.37	0.42	0.46	0.46	0.40	0.39	0.39
Yb	2.31	2.15	2.45	2.61	2.65	2.26	2.23	2.22
Lu	0.34	0.32	0.35	0.38	0.40	0.34	0.32	0.33
Hf	7.52	6.97	7.88	8.58	8.69	7.57	7.48	7.54
Ta	5.54	4.82	6.23	7.50	7.59	6.02	5.92	5.90
Pb	3.27	2.63	3.64	4.38	2.76	3.46	3.55	3.33
Th	7.30	6.24	8.30	10.17	10.31	8.22	8.11	7.97
U	1.76	1.50	2.07	2.50	2.56	2.01	2.00	1.96

Table 3. Olivine-clinopyroxene pairs and temperatures calculated after Loucks (1996)

Year:	1954	1954	1954	1954	1954	1954	1954	1954
Analysis:	54-115	54-26	54-25	54-29	54-24	54-21	54-23	54-22
(wt.%)								
SiO_2	38.81	38.76	38.95	38.76	38.92	38.99	39.15	38.91
FeO	20.40	20.27	19.60	20.14	20.03	20.25	20.47	19.97
MnO	0.48	0.43	0.43	0.42	0.41	0.43	0.43	0.41
MgO	40.17	40.39	41.15	40.51	40.54	40.73	40.63	40.47
NiO	0.05	0.05	0.05	0.05	0.06	0.05	0.03	0.02
CaO	0.30	0.30	0.31	0.30	0.28	0.31	0.30	0.30
Total	100.21	100.18	100.48	100.18	100.26	100.77	101.03	100.09
Mg#	77.83	78.03	78.92	78.19	78.30	78.20	77.96	78.32
Analysis:	54-AP1	54CP26	54-CP27	54-CP16	54-CP231	54-CP34	54-CP230	54-CP33
(wt.%)								
SiO_2	49.05	46.63	47.37	48.30	47.95	48.80	47.84	48.52
TiO_2	1.95	2.71	2.52	2.25	2.54	2.20	2.61	2.36
Al_2O_3	4.84	7.70	7.02	5.58	6.48	5.81	6.41	5.65
Cr_2O_3	0.00	0.02	0.17	0.00	0.07	0.27	0.06	0.10
FeO	6.57	7.12	6.99	6.77	7.13	6.48	6.94	6.57
MnO	0.16	0.14	0.11	0.17	0.14	0.11	0.17	0.14
MgO	13.33	12.58	12.65	13.07	12.58	13.23	12.97	13.05
NiO	0.01	0.01	0.00	0.00	0.01	0.00	0.01	0.02
CaO	22.74	22.98	23.13	22.80	22.60	23.36	22.83	23.01
Na_2O	0.43	0.51	0.41	0.51	0.59	0.40	0.50	0.45
Total	99.07	100.38	100.37	99.45	100.08	100.65	100.33	99.85
X_{Fe}	0.1105	0.1207	0.1181	0.1142	0.1218	0.1080	0.1171	0.1108
X_{Mg}	0.3995	0.3802	0.3812	0.3930	0.3832	0.3931	0.3898	0.3922
X_{Ca}	0.4900	0.4991	0.5007	0.4928	0.4949	0.4989	0.4931	0.4970
T (^oC)	1,162	1,099	1,159	1,142	1,181	1,144	1,139	1,165

Table 3. Continued

Year:	1954	1954	1959	1959	1959	1982	1982	1982
Analysis:	54-20	54-27	59-O20	59-O21	59-O22	82-3ao8	82-3ao9	82-3ao10
(wt.%)								
SiO_2	38.91	39.26	39.92	38.97	39.11	39.11	38.74	39.02
FeO	20.17	20.32	19.92	19.48	19.50	18.74	18.58	18.59
MnO	0.41	0.40	0.32	0.33	0.31	0.29	0.29	0.30
MgO	40.61	41.09	40.86	40.88	41.73	41.98	42.05	41.38
NiO	0.03	0.02	0.10	0.08	0.10	0.16	0.10	0.13
CaO	0.30	0.28	0.39	0.39	0.37	0.35	0.36	0.35
Total	100.43	101.37	100.50	100.13	101.12	100.63	100.13	99.79
Mg#	78.21	78.28	78.52	78.91	79.23	79.97	80.14	79.87
Analysis:	54-CP36	54-CP21	59-3CP66	59-3CP61	59-3CP60	82-3ap44	82-3ap55	82-3ap54
(wt.%)								
SiO_2	48.25	45.97	43.15	43.05	42.39	43.07	48.40	48.63
TiO_2	2.33	2.66	4.32	4.25	4.20	3.98	2.23	2.10
Al_2O_3	6.13	7.14	9.53	9.80	10.28	10.06	5.87	5.50
Cr_2O_3	0.27	0.12	0.03	0.09	0.08	0.01	0.00	0.06
FeO	6.76	7.29	9.15	8.65	8.78	8.74	7.59	7.67
MnO	0.10	0.01	0.11	0.11	0.10	0.10	0.12	0.13
MgO	13.16	12.40	10.44	10.70	10.48	10.56	13.05	13.20
NiO	0.03	0.00	0.00	0.00	0.02	0.02	0.03	0.03
CaO	23.23	22.72	22.49	22.68	22.56	22.52	22.71	22.48
Na_2O	0.49	0.50	0.45	0.45	0.41	0.51	0.30	0.35
Total	100.73	98.81	99.67	99.78	99.29	99.56	100.30	100.14
X_{Fe}	0.1127	0.1246	0.1617	0.1524	0.1557	0.1549	0.1266	0.1279
X_{Mg}	0.3911	0.3779	0.3291	0.3359	0.3314	0.3338	0.3880	0.3922
X_{Ca}	0.4962	0.4976	0.5092	0.5118	0.5129	0.5113	0.4854	0.4799
T (^oC)	1,110	1,103	1,251	1,211	1,216	1,229	1,226	1,218

Table 3. Continued								
Year:	1982	1982	1982	1982	1982	1982	1999	1999
Analysis:	82-3ao11	82-3ao12	82-3ao13	82-3ao14	82-3Co23	82-3Co24	99-4a11	99-4a12
(wt.%)								
SiO_2	38.95	38.97	38.98	39.03	38.96	39.15	39.93	39.63
FeO	18.43	17.93	19.10	18.40	19.17	19.26	14.82	15.09
MnO	0.30	0.30	0.30	0.29	0.31	0.32	0.26	0.26
MgO	41.85	41.84	41.73	41.86	41.04	40.75	44.91	44.68
NiO	0.15	0.16	0.11	0.14	0.13	0.07	0.17	0.17
CaO	0.35	0.34	0.38	0.35	0.41	0.40	0.33	0.32
Total	100.05	99.55	100.62	100.08	100.03	99.95	100.43	100.16
Mg#	80.19	80.62	79.57	80.22	79.24	79.04	84.38	84.07
Analysis:	82-3ap53	82-3ap45	82-3ap46	82-3ap47	82-3cp64	82-3cp65	99-4ap21	99-4ap24
(wt.%)								
SiO_2	43.40	43.79	42.91	42.79	43.37	43.43	41.49	47.39
TiO_2	4.06	3.73	4.04	4.19	4.35	4.00	5.29	2.34
Al_2O_3	9.63	9.62	10.01	10.52	9.69	10.06	10.97	6.70
Cr_2O_3	0.03	0.04	0.05	0.07	0.20	0.03	0.02	0.05
FeO	8.76	8.57	8.96	8.78	8.92	8.76	9.16	7.13
MnO	0.11	0.11	0.12	0.11	0.09	0.11	0.13	0.11
MgO	10.46	11.05	10.59	10.65	10.59	10.70	10.55	13.28
NiO	0.03	0.03	0.00	0.01	0.04	0.03	0.00	0.09
CaO	22.59	22.59	22.59	22.65	22.41	22.62	21.88	22.87
Na_2O	0.43	0.47	0.43	0.46	0.45	0.43	0.56	0.43
Total	99.50	100.01	99.68	100.23	100.10	100.14	100.04	100.38
X_{Fe}	0.1555	0.1498	0.1577	0.1546	0.1578	0.1542	0.1637	0.1186
X_{Mg}	0.3308	0.3443	0.3325	0.3344	0.3340	0.3357	0.3357	0.3939
X_{Ca}	0.5137	0.5059	0.5097	0.5110	0.5082	0.5101	0.5007	0.4875
T (°C)	1,276	1,220	1,226	1,217	1,264	1,232	1,296	1,172

Table 3. Continued

Year:	1999	1999	1999	1999	1999	2000	2000	2000
Analysis:	99-4a13	99-4a21	99-4a22	99-4a42	99-4a43	2000-5b11	2000-5b12	2000-5b13
(wt.%)								
SiO_2	39.76	39.87	39.52	39.95	39.96	40.00	40.06	39.98
FeO	14.90	14.78	14.88	13.86	13.99	15.29	15.19	14.95
MnO	0.25	0.24	0.25	0.22	0.20	0.23	0.26	0.25
MgO	44.42	44.91	44.85	45.60	45.35	44.26	44.53	43.96
NiO	0.15	0.18	0.15	0.23	0.19	0.18	0.17	0.14
CaO	0.33	0.33	0.34	0.31	0.30	0.33	0.32	0.32
Total	99.81	100.32	100.01	100.20	100.04	100.30	100.53	99.63
Mg#	84.17	84.42	84.31	85.44	85.25	83.76	83.93	83.98
Analysis:	99-4ap25	99-4ap30	99-4ap31	99-4ap32	99-4ap28	2000-5bp13	2000-5bp12	2000-5bp17
(wt.%)								
SiO_2	47.68	48.96	44.17	44.88	48.41	44.41	44.25	45.55
TiO_2	2.31	2.10	4.20	3.88	2.21	2.62	3.97	3.19
Al_2O_3	6.29	4.75	8.84	8.34	5.49	7.05	9.07	8.02
Cr_2O_3	0.01	0.01	0.00	0.01	0.00	0.01	0.00	0.00
FeO	6.87	8.00	8.53	8.21	7.75	7.34	7.97	7.94
MnO	0.16	0.21	0.19	0.17	0.19	0.15	0.13	0.15
MgO	13.43	14.14	11.51	11.93	13.61	12.49	11.73	11.86
NiO	0.02	0.00	0.04	0.00	0.02	0.03	0.04	0.00
CaO	22.61	21.62	22.15	22.15	21.72	22.51	22.08	22.35
Na_2O	0.42	0.36	0.54	0.52	0.40	0.51	0.55	0.44
Total	99.80	100.12	100.18	100.09	99.79	97.12	99.78	99.49
X_{Fe}	0.1149	0.1313	0.1485	0.1418	0.1295	0.1256	0.1393	0.1375
X_{Mg}	0.4005	0.4139	0.3572	0.3677	0.4054	0.3809	0.3658	0.3663
X_{Ca}	0.4846	0.4548	0.4943	0.4905	0.4651	0.4935	0.4948	0.4962
T (^oC)	1,193	1,265	1,284	1,292	1,295	1,014	1,252	1,286

Table 3. Continued

Year:	2000	2000	2000
Analysis:	2000-5b14	2000-5b15	2000-5b16
(wt.%)			
SiO_2	39.77	39.79	39.78
FeO	15.05	15.13	15.27
MnO	0.25	0.23	0.24
MgO	43.69	44.02	44.03
NiO	0.17	0.17	0.14
CaO	0.31	0.30	0.34
Total	99.23	99.67	99.81
Mg#	83.80	83.83	83.72
Analysis:	2000-5bp18	2000-5bp19	2000-5bp21
(wt.%)			
SiO_2	48.43	47.39	48.71
TiO_2	2.11	2.57	1.69
Al_2O_3	5.59	6.88	5.78
Cr_2O_3	0.03	0.02	0.01
FeO	6.83	7.66	7.48
MnO	0.15	0.12	0.22
MgO	13.61	12.82	12.78
NiO	0.02	0.04	0.00
CaO	22.70	22.43	22.39
Na_2O	0.42	0.47	0.49
Total	99.87	100.40	99.55
X_{Fe}	0.1134	0.1293	0.1269
X_{Mg}	0.4033	0.3857	0.3865
X_{Ca}	0.4833	0.4850	0.4866
T (^oC)	1,200	1,182	1,282

Table 4. Average compositions of mineral cores in spinel harzburgite SI2000/4

Cores	Olivine (n=6)	Orthopyr. (n=6)	Clinopyr. (n=6)	Spinel (n=9)
SiO2	40.90	55.43	52.31	0.19
TiO2		0.11	0.48	0.13
Al2O3		4.17	6.80	54.83
Cr2O3		0.39	0.92	12.10
FeO	9.85	6.25	2.42	10.67
MnO	0.13	0.14	0.08	0.12
MgO	49.41	33.29	14.75	20.94
NiO	0.40	0.12	0.08	0.36
CaO	0.056	0.48	20.02	
Na2O		0.07	1.74	
Total	100.75	100.38	97.86	99.34
s.d.				
SiO2	0.08	0.15	0.12	0.02
TiO2		0.01	0.03	0.02
Al2O3		0.05	0.05	0.46
Cr2O3		0.02	0.03	0.61
FeO	0.18	0.09	0.05	0.14
MnO	0.03	0.02	0.04	0.02
MgO	0.15	0.17	0.08	0.10
NiO	0.01	0.01	0.01	0.01
CaO	0.006	0.03	0.08	
Na2O		0.02	0.02	
Mg#	89.94	90.47	91.58	77.77
T_{BKN} (^{o}C)	1,019			
P_{KB} (kb)	13.3			

Table 5. Characteristics of glass inclusions.

Inclusion	Shape	Size (microns)	Vapor bubble diameter (microns)	Vapor bubble vol %	Crystals
SI54-1C	Spherical	192			None
SI54-1D	Spherical	144	36	1.6	Spinel
SI54-1F1	Triangular prism	120, 84, 96	28	2.3	
SI54-1F2	Irregular	144, 120, 90			Spinel
SI54-1G	Spherical	96			Spinel
SI59-1A	Elongated	192, 120, 120	36	1.9	sulfides
SI59-1C	Spherical	72	24	3.7	sulfides, spinel
SI59-1D	Elongated	82, 50, 50	30	13.2	sulfide
SI82-3A	Elongated	216, 192, 190	38	0.7	Spinel
SI82-3B	Elongated	144, 110, 120	24	0.7	None
SI82-3C1	Irregular	120, 60, 40	36	16.2	None
SI82-3C2	Spherical	40			None
SI82-3C3	Spherical	40	10	1.6	None
SI82-3C4	Spherical	30			None
SI82-3C5	Irregular	48, 43, 45	10	1.1	Minor spinel
SI99-4A1	Elongated	130, 90, 90	48	10.5	None
SI99-4A2	Spherical	72			None
SI2000-5A	Elongated	144, 120, 120	34	1.9	None
SI2000-5B	Elongated	190, 62, 62	36	6.4	Spinel
SI2000-5C	Rod	168, 120	24	0.6	Spinel
SI2000-5D	Spherical	86	24	3.6	None
SI2000-5E1	Spherical	72			None
SI2000-5E2	Spherical	190	96	12.9	Spinel
SI2000-5E3	Elongated	240, 120, 120	52	3.8	None
SI2000-5F	Spherical	120	24	0.6	Spinel

SI2000-5H	Spherical	180	56	3	Spinel

Table 6. Glass inclusion and host olivine compositions, plus corrections for host-olivine precipitation.

Year:	1954	1954	1954	1954	1954	1959	1959
Glass Inclusion:	54-1C	54-1D	54-1F1	54-1F2	54-1G	59-1A	59-1C
Spots analyzed:	3	3	1	1	2	6	2
mean (wt.%)							
SiO_2	47.83	51.26	46.35	45.60	45.75	43.33	44.10
TiO_2	2.28	2.83	3.31	3.63	3.19	3.49	3.13
Al_2O_3	19.91	14.92	15.85	15.97	16.58	14.73	14.94
FeO^t	7.40	9.16	8.46	9.48	11.18	11.02	9.99
MnO	0.15	0.16	0.14	0.18	0.15	0.19	0.20
MgO	3.18	4.85	5.14	4.28	6.07	4.89	4.67
CaO	7.34	8.19	13.81	15.68	8.40	13.59	13.84
Na_2O	6.61	6.02	3.50	3.32	4.57	3.58	3.81
K_2O	3.12	0.66	0.70	0.32	1.93	1.42	1.89
P_2O_5	1.48	0.53	0.66	0.73	0.88	0.72	0.99
SO_3^t	0.30	0.12	0.39	0.55	0.41	0.60	0.71
Cl	0.25	0.06	0.11	0.11	0.14	0.13	0.17
Total	99.83	98.76	98.43	99.84	99.26	97.68	98.43
H_2O by difference	0.0	1.1	1.4	0.0	0.6	2.1	1.4
1 s.d.							
SiO_2	1,74	0.24			0.91	0.46	0.54
TiO_2	0.02	0.03			0.09	0.03	0.02
Al_2O_3	0.21	0.41			0.65	0.12	0.14
FeO^t	0.45	0.65			0.05	0.15	0.29
MnO	0.01	0.07			0.04	0.03	0.06
MgO	0.19	0.55			0.15	0.09	0.01
CaO	0.44	0.17			0.05	0.25	0.10
Na_2O	0.17	0.03			0.04	0.05	0.00
K_2O	0.09	0.03			0.03	0.03	0.05
P_2O_5	0.07	0.04			0.03	0.04	0.06
SO_3^t	0.00	0.10			0.06	0.01	0.00
Cl	0.01	0.00			0.00	0.00	0.00
$\%S^{6+}$	17		14	36	6	41	23
Host olivine:	SI54-1C	SI54-1D	SI54-1F1	SI54-1F2	SI54-1G	SI59-1A	SI59-1C
spots:	3	3	2	2	3	6	3
mean (wt.%)							
SiO_2	39.87	38.71	39.62	39.22	38.54	38.78	39.37
FeO	16.89	16.75	15.22	15.35	19.93	18.72	17.23
MnO	0.32	0.33	0.25	0.26	0.40	0.32	0.31
MgO	43.38	42.79	44.36	44.24	40.64	41.49	42.43
NiO	0.14	0.14	0.17	0.18	0.05	0.15	0.11
CaO	0.40	0.36	0.38	0.37	0.35	0.43	0.55
Total	101.01	99.08	100.01	99.61	99.91	99.90	99.99
1 s.d.							
SiO_2	0.19	0.52	0.25	0.21	0.13	0.37	0.15
FeO	0.20	0.30	0.37	0.31	0.20	0.12	0.08
MnO	0.02	0.02	0.01	0.01	0.02	0.01	0.03
MgO	0.33	0.34	0.13	0.05	0.19	0.22	0.15
NiO	0.02	0.04	0.04	0.00	0.03	0.01	0.01
CaO	0.02	0.01	0.02	0.01	0.00	0.03	0.10
Mg#	82.07	82.00	83.86	83.71	78.43	79.80	81.44
Olivine-corrected glass analysis:							
Glass Inclusion:	54-1C	54-1D	54-1F1	54-1F2	54-1G	59-1A	59-1C
Olivine added (wt.%):	5	4	4	8	0	5	5
SiO_2	47.49	51.39	46.79	45.17	46.10	44.08	44.53
TiO_2	2.17	2.75	3.23	3.34	3.22	3.39	3.02
Al_2O_3	18.94	14.50	15.46	14.71	16.70	14.33	14.42
FeO^t	7.88	9.58	8.86	9.97	11.27	11.65	10.50
MnO	0.16	0.17	0.15	0.18	0.15	0.20	0.20
MgO	5.17	6.44	6.79	7.49	6.11	6.83	6.63

Table 6. Continued

Year:	1959	1982	1982	1982	1982	1982	1982
Glass Inclusion:	59-1D	82-3A	82-3B	82-3C1	82-3C2	82-3C3	82-3C4
Spots analyzed:	3	5	3	1	2	1	1
mean (wt.%)							
SiO_2	42.69	42.26	44.15	44.12	43.98	43.58	42.74
TiO_2	3.62	3.58	3.18	3.33	3.30	3.36	3.33
Al_2O_3	15.60	14.50	14.74	14.20	14.32	14.54	14.26
FeO^t	10.11	11.92	11.67	12.36	12.13	12.45	11.97
MnO	0.17	0.20	0.20	0.21	0.18	0.17	0.20
MgO	4.57	5.79	5.39	5.81	5.72	5.68	5.47
CaO	13.27	12.39	12.28	11.95	12.04	11.55	11.79
Na_2O	3.80	3.40	3.62	3.44	3.29	3.26	3.47
K_2O	1.92	1.66	1.40	1.24	1.25	1.20	1.18
P_2O_5	0.91	0.89	0.51	0.51	0.49	0.54	0.52
SO_3^t	0.71	0.66	0.49	0.47	0.47	0.47	0.47
Cl	0.16	0.15	0.11	0.10	0.10	0.11	0.10
Total	97.54	97.38	97.73	97.73	97.27	96.90	95.51
H_2O by difference	2.3	2.4	2.1	2.1	2.5	2.9	4.3
1 s.d.							
SiO_2	0.28	0.65	0.40		0.05		
TiO_2	0.04	0.03	0.06		0.02		
Al_2O_3	0.04	0.27	0.09		0.00		
FeO^t	0.32	0.10	0.66		0.11		
MnO	0.05	0.01	0.06		0.02		
MgO	0.13	0.23	0.15		0.02		
CaO	0.08	0.33	0.81		0.01		
Na_2O	0.02	0.12	0.31		0.13		
K_2O	0.01	0.14	0.08		0.01		
P_2O_5	0.04	0.06	0.03		0.04		
SO_3^t	0.00	0.01	0.01		0.01		
Cl	0.00	0.00	0.01		0.01		
$\%S^{6+}$	33	31	21	49			
Host olivine:	SI59-1D	SI82-3A	SI82-3B	SI82-3C1	SI82-3C2	SI82-3C3	SI-82-3C4
spots:	5	5	5	2	3	2	2
mean (wt.%)							
SiO_2	38.75	39.09	38.71	38.96	38.86	39.07	38.87
FeO	16.52	17.32	18.06	18.07	18.09	18.00	18.21
MnO	0.28	0.29	0.31	0.25	0.27	0.30	0.30
MgO	43.32	42.78	42.55	42.20	42.30	42.19	42.31
NiO	0.13	0.16	0.16	0.17	0.16	0.15	0.17
CaO	0.41	0.40	0.37	0.39	0.39	0.38	0.37
Total	99.41	100.04	100.15	100.05	100.07	100.10	100.23
1 s.d.							
SiO_2	1.12	0.24	0.29	0.03	0.13	0.48	0.10
FeO	0.12	0.17	0.14	0.06	0.03	0.10	0.04
MnO	0.01	0.01	0.02	0.04	0.04	0.00	0.02
MgO	0.29	0.25	0.16	0.31	0.12	0.17	0.01
NiO	0.02	0.02	0.02	0.01	0.02	0.03	0.02
CaO	0.01	0.02	0.01	0.02	0.02	0.02	0.02
Mg#	82.38	81.49	80.77	80.63	80.65	80.69	80.56
Olivine-corrected glass analysis:							
Glass Inclusion:	59-1D	82-3A	82-3B	82-3C1	82-3C2	82-3C3	82-3C4
Olivine added (wt.%):	7	6	6	5	5	6	6
SiO_2	43.43	43.13	44.78	44.83	44.90	44.61	44.39
TiO_2	3.45	3.46	3.05	3.23	3.22	3.26	3.28
Al_2O_3	14.87	14.00	14.18	13.80	13.98	14.11	14.04
FeO^t	10.80	12.54	12.30	12.92	12.75	13.16	12.87
MnO	0.19	0.21	0.21	0.22	0.19	0.18	0.21
MgO	7.41	8.16	7.73	7.76	7.70	8.04	7.92

Table 6. Continued

Year:	1982	1999	1999	2000	2000	2000	2000
Glass Inclusion:	82-3C5	99-4A1	99-4A2	2000-5A	2000-5B	2000-5C	2000-5D
Spots analyzed:	1	3	2	4	6	3	2
mean (wt.%)							
SiO_2	42.87	47.14	44.07	45.98	45.88	45.21	46.53
TiO_2	3.45	3.51	3.93	3.44	3.00	3.78	3.56
Al_2O_3	15.15	16.21	15.48	15.38	14.25	15.08	15.98
FeO^t	12.64	11.06	11.94	11.80	9.93	11.69	11.84
MnO	0.21	0.22	0.21	0.24	0.17	0.24	0.22
MgO	5.02	4.75	5.11	4.91	5.29	5.00	4.70
CaO	12.26	9.47	11.23	9.48	12.83	10.41	8.12
Na_2O	3.50	4.45	3.30	4.13	3.65	4.27	4.73
K_2O	1.36	0.93	1.44	1.50	1.48	1.40	1.92
P_2O_5	0.61	0.59	0.63	0.69	0.45	0.68	0.73
SO_3^t	0.47	0.48	0.46	0.47	0.56	0.49	0.45
Cl	0.10	0.09	0.12	0.12	0.11	0.10	0.14
Total	97.62	98.91	97.89	98.14	97.60	98.34	98.92
H_2O by difference	2.2	0.9	1.9	1.7	2.2	1.5	0.9
1 s.d.							
SiO_2		0.82	1.40	0.30	0.19	0.06	0.06
TiO_2		0.11	0.09	0.04	0.04	0.03	0.06
Al_2O_3		0.31	0.23	0.15	0.17	0.23	0.12
FeO^t		0.71	0.13	0.32	0.29	0.16	0.17
MnO		0.04	0.02	0.02	0.03	0.04	0.01
MgO		0.16	0.13	0.13	0.34	0.14	0.00
CaO		0.41	1.40	0.10	0.14	0.09	0.07
Na_2O		0.38	0.86	0.07	0.21	0.08	0.20
K_2O		0.21	0.27	0.03	0.03	0.02	0.03
P_2O_5		0.04	0.02	0.05	0.02	0.04	0.04
SO_3^t		0.12	0.01	0.00	0.00	0.00	0.00
Cl		0.02	0.01	0.00	0.00	0.00	0.00
$\%S^{6+}$		-2		44	38	51	39
Host olivine:	SI82-3C5	SI99-4A1	SI99-4A2	SI2000-5A	SI2000-5B	SI2000-5C	SI2000-5D
spots:	3	3	3	4	5	3	4
mean (wt.%)							
SiO_2	38.89	37.68	38.17	38.49	39.10	38.96	38.42
FeO	18.07	19.93	19.73	20.36	16.61	19.73	20.03
MnO	0.27	0.36	0.38	0.36	0.25	0.36	0.43
MgO	42.24	40.61	40.63	40.51	43.01	40.87	40.76
NiO	0.17	0.09	0.11	0.11	0.15	0.12	0.11
CaO	0.39	0.35	0.33	0.36	0.57	0.37	0.26
Total	100.02	99.02	99.35	100.19	99.68	100.42	100.01
1 s.d.							
SiO_2	0.13	1.55	0.30	0.31	0.63	0.16	0.28
FeO	0.05	0.23	0.26	0.14	0.15	0.18	0.06
MnO	0.04	0.02	0.02	0.01	0.03	0.03	0.03
MgO	0.23	0.26	0.16	0.31	0.53	0.38	0.25
NiO	0.01	0.02	0.01	0.02	0.03	0.01	0.01
CaO	0.02	0.01	0.02	0.03	0.13	0.05	0.02
Mg#	80.65	78.41	78.60	78.01	82.19	78.69	78.39
Olivine-corrected glass analysis:							
Glass Inclusion:	82-3C5	99-4A1	99-4A2	2000-5A	2000-5B	2000-5C	2000-5D
Olivine added (wt.%):	8	4	4	4	4	4	5
SiO_2	43.51	47.28	44.75	46.52	46.70	45.69	46.61
TiO_2	3.25	3.41	3.85	3.37	2.95	3.69	3.42
Al_2O_3	14.28	15.74	15.18	15.05	14.02	14.72	15.35
FeO^t	13.35	11.54	12.50	12.36	10.43	12.20	12.37
MnO	0.21	0.23	0.22	0.25	0.17	0.24	0.23
MgO	8.11	6.25	6.65	6.42	6.93	6.51	6.55

Table 6. Continued

Year:	2000	2000	2000	2000	2000
Glass Inclusion:	2000-5E1	2000-5E2	2005-5E3	2000-5F	2000-5H
Spots analyzed:	2	5	1	1	5
mean (wt.%)					
SiO_2	46.60	45.10	45.34	44.75	45.52
TiO_2	3.08	3.28	3.41	3.67	3.33
Al_2O_3	15.61	15.02	15.71	15.27	15.28
FeO^t	11.16	12.32	12.17	11.83	12.31
MnO	0.22	0.22	0.20	0.22	0.20
MgO	4.79	4.99	4.88	5.10	4.94
CaO	9.62	9.67	9.77	10.15	10.14
Na_2O	4.18	3.90	4.18	4.20	4.04
K_2O	1.58	1.52	1.57	1.60	1.41
P_2O_5	0.63	0.83	0.75	0.60	0.71
SO_3^t	0.43	0.40	0.43	0.48	0.45
Cl	0.13	0.12	0.14	0.11	0.11
Total	98.04	97.37	98.52	97.98	98.42
H_2O by difference	1.8	2.4	1.3	1.8	1.4
1 s.d.					
SiO_2	0.32	0.14			0.26
TiO_2	0.02	0.05			0.03
Al_2O_3	0.16	0.11			0.20
FeO^t	0.15	0.31			0.34
MnO	0.02	0.03			0.03
MgO	0.03	0.09			0.11
CaO	0.13	0.20			0.15
Na_2O	0.14	0.18			0.10
K_2O	0.07	0.05			0.02
P_2O_5	0.01	0.37			0.04
SO_3^t	0.01	0.04			0.00
Cl	0.00	0.01			0.00
$\%S^{6+}$	43			41	34
Host olivine:	SI2000-5E1	SI2000-5E2	SI2005-5E3	SI2000-5F	SI2000-5H
spots:	3	3	2	4	4

mean (wt.%)					
SiO_2	38.19	38.22	38.16	38.63	38.59
FeO	20.68	20.66	20.54	20.02	20.54
MnO	0.35	0.35	0.36	0.35	0.38
MgO	40.16	40.30	40.52	40.83	39.94
NiO	0.10	0.12	0.13	0.10	0.13
CaO	0.34	0.34	0.35	0.34	0.45
Total	99.83	99.99	100.06	100.26	100.02
1 s.d.					
SiO_2	0.27	0.39	0.53	0.13	0.41
FeO	0.11	0.50	0.64	0.22	0.14
MnO	0.02	0.02	0.02	0.04	0.02
MgO	0.52	0.40	0.18	0.17	0.64
NiO	0.00	0.02	0.02	0.03	0.03
CaO	0.02	0.02	0.02	0.00	0.15
Mg#	77.59	77.66	77.86	78.43	77.61
Olivine-corrected glass analysis:					
Glass Inclusion:	2000-5E1	2000-5E2	2005-5E3	2000-5F	2000-5H
Olivine added (wt.%):	3	4	5	4	4
SiO_2	47.26	45.99	45.62	45.38	45.94
TiO_2	3.05	3.23	3.29	3.59	3.25
Al_2O_3	15.44	14.81	15.15	14.96	14.90
FeO^t	11.66	12.98	12.76	12.39	12.83
MnO	0.23	0.23	0.21	0.23	0.21
MgO	5.95	6.53	6.73	6.62	6.41
CaO	9.53	9.55	9.43	9.96	9.91
Na_2O	4.13	3.84	4.03	4.12	3.94
K_2O	1.56	1.50	1.51	1.57	1.37
P_2O_5	0.62	0.82	0.72	0.59	0.70
SO_3^t	0.43	0.39	0.41	0.47	0.43
Cl	0.13	0.12	0.13	0.11	0.11
Total	100.00	100.00	99.99	100.00	99.99
T^oC Sug-anhy	1,159	1,171	1,175	1,173	1,169
T^oC Sug-hyd	1,127	1,140	1,144	1,142	1,137

Table 7. Volatiles in glass by FTIR and SIMS with EMP comparisons

Year:	1959	2000	2000	2000
Glass inclusion:	59-1A	2000-5A	2000-5C	2000-5F
FTIR				
Thickness (microns):	77	66	90	77
Glass density (g/L):	2807	2759	2774	2778
Total water from absorbance at 3535 cm^{-1}				
Rel. Peak Ht. (Abs. units)	0.82	0.70	1.07	1.08
Molar absorptivity (L/mol-cm)	63	63	63	63
Total H_2O (wt.%)	1.09	1.10	1.22	1.44
Molecular H_2O from absorbance at 1635 cm^{-1}				
Rel. Peak Ht. (Abs. units)	0.045	0.04	0.062	0.084
Molar absorptivity (L/mol-cm)	15.9	20.0	18.2	18.1
Molecular H_2O (wt.%)	0.24	0.20	0.25	0.39
CO_2 from 1515 cm^{-1} peak				
Absorbance	0.120	0.081	0.135	0.133
e1515 (L/mol-cm)	279	279	279	279
CO_2 (ppm)	876	703	853	981
CO_2 from 1435 cm^{-1} peak				
Absorbance	0.12	0.086	0.124	0.133
e1435 (L/mol-cm)	279	279	279	279
CO_2 (ppm)	876	743	785	981
SIMS and comparisons				
H_2O SIMS (wt.%)	1.66	1.70	1.65	
H_2O FTIR (wt.%)	1.09	1.10	1.22	1.44
H_2O by EMP difference (wt.%)	2.14	1.66	1.46	1.82
CO_2 SIMS (ppm)	967	683	752	
CO_2 FTIR avg (ppm)	876	723	819	981
F SIMS (ppm)	1530	1770	1983	

S SIMS (ppm)	3096	2619	2947	
S EMP (ppm)	2411	1882	1966	1902
Cl SIMS (ppm)	1031	1070	983	
Cl EMP (ppm)	1270	1150	980	1130
Pressure and depth estimates				
Pressure (bars)	958	964	931	
Depth (km)	3.45	3.47	3.35	

Table 8. LA-ICP-MS analyses of glass inclusions.

Inclusion:	Isotope	SI2000-5C	1 s.d.	SI2000-5F	1 s.d.	SI59-1A	1 s.d.
Spot (microns):		30		55		55	
CaO (wt.%)	^{43}Ca	10.41	0.10	10.15	0.05	13.59	0.09
TiO_2 (wt.%)	^{49}Ti	4.92	0.01	4.64	0.01	4.63	0.01
MnO (wt.%)	^{55}Mn	0.24	0.00	0.23	0.00	0.18	0.00
Ni (ppm)	^{62}Ni	58.0	2.7	46.5	1.3	45.7	2.0
Rb (ppm)	^{85}Rb	39.2	0.5	37.8	0.3	39.9	0.5
Sr (ppm)	^{86}Sr	932	7	855	3	1070	6
Y (ppm)	^{89}Y	38.7	0.5	35.1	0.2	42.3	0.5
Zr (ppm)	^{90}Zr	364.4	2.0	349.6	1.0	442.6	2.1
Nb (ppm)	^{93}Nb	80.6	0.6	85.4	0.4	101.3	0.6
Cs (ppm)	^{133}Cs	0.50	0.04	0.41	0.02	0.49	0.03
Ba (ppm)	^{137}Ba	381	3	387	2	384	3
La (ppm)	^{139}La	59.2	0.4	62.5	0.2	73.9	0.4
Ce (ppm)	^{140}Ce	117.8	0.6	125.3	0.3	130.6	0.5
Nd (ppm)	^{146}Nd	60.7	1.0	60.1	0.5	64.6	0.9
Sm (ppm)	^{147}Sm	10.53	0.45	11.04	0.24	11.59	0.42
Eu (ppm)	^{153}Eu	3.10	0.12	3.19	0.07	3.63	0.12
Gd (ppm)	^{157}Gd	10.13	0.44	9.39	0.23	10.71	0.43
Tb (ppm)	^{159}Tb	1.44	0.06	1.18	0.03	1.50	0.06
Ho (ppm)	^{165}Ho	1.43	0.07	1.22	0.03	1.38	0.06
Er (ppm)	^{167}Er	3.48	0.15	3.15	0.08	3.53	0.15
Yb (ppm)	^{172}Yb	3.00	0.20	2.49	0.10	2.84	0.19
Lu (ppm)	^{175}Lu	0.39	0.03	0.36	0.02	0.38	0.03
Hf (ppm)	^{178}Hf	7.85	0.25	7.60	0.13	8.53	0.25
Ta (ppm)	^{181}Ta	5.31	0.12	5.74	0.06	6.12	0.12
Pb (ppm)	^{208}Pb	3.31	0.13	3.90	0.07	3.81	0.11
Th (ppm)	^{232}Th	6.55	0.12	7.59	0.07	9.28	0.13
U (ppm)	^{238}U	1.72	0.05	1.93	0.03	1.73	0.04

The LA-ICP-MS data were normalized to CaO concentrations determined by electron microprobe (Table 6).

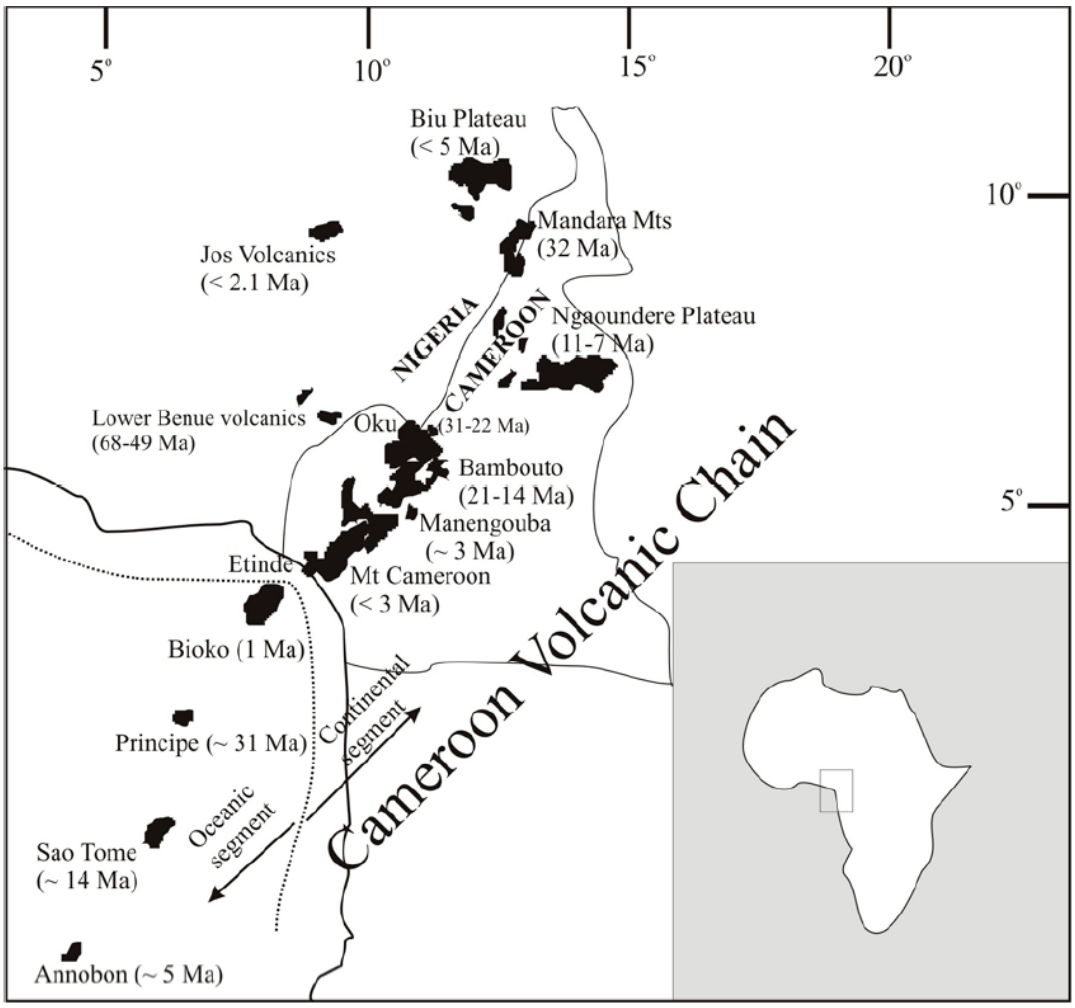

Suh et al. – Fig. 1

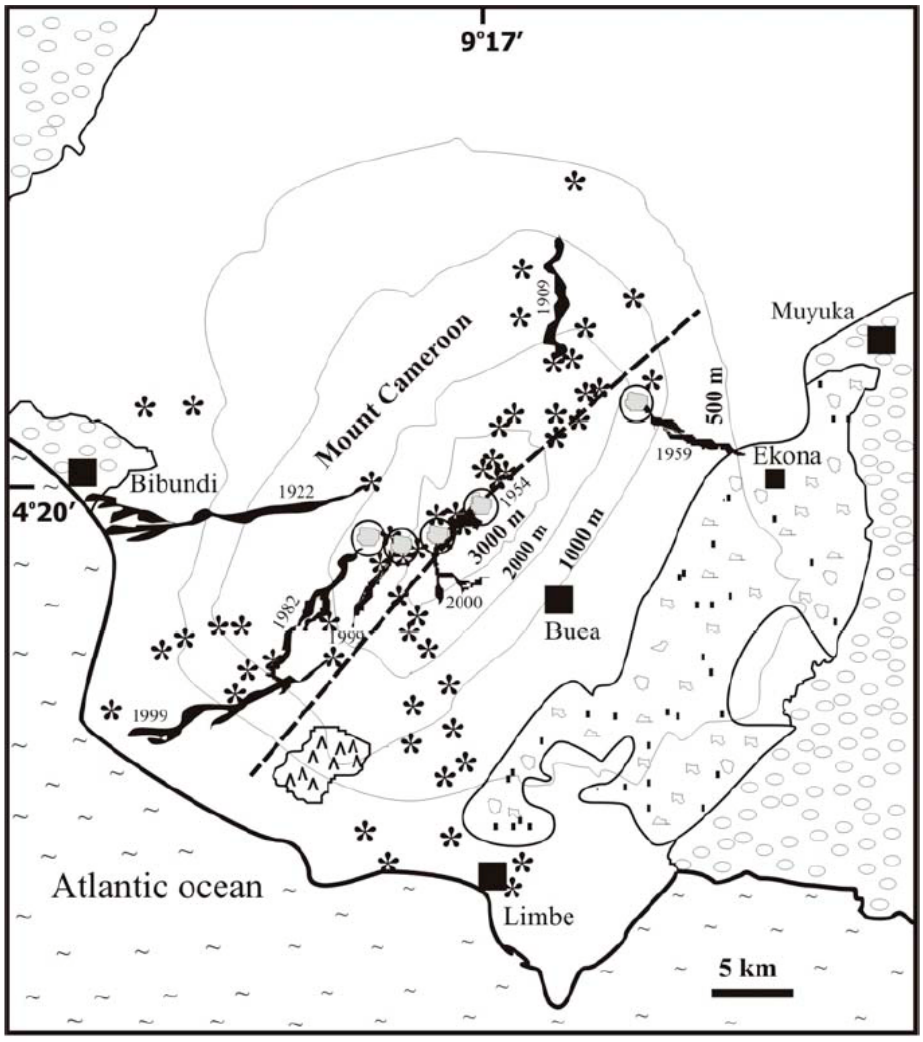

Suh et al. – Fig. 2

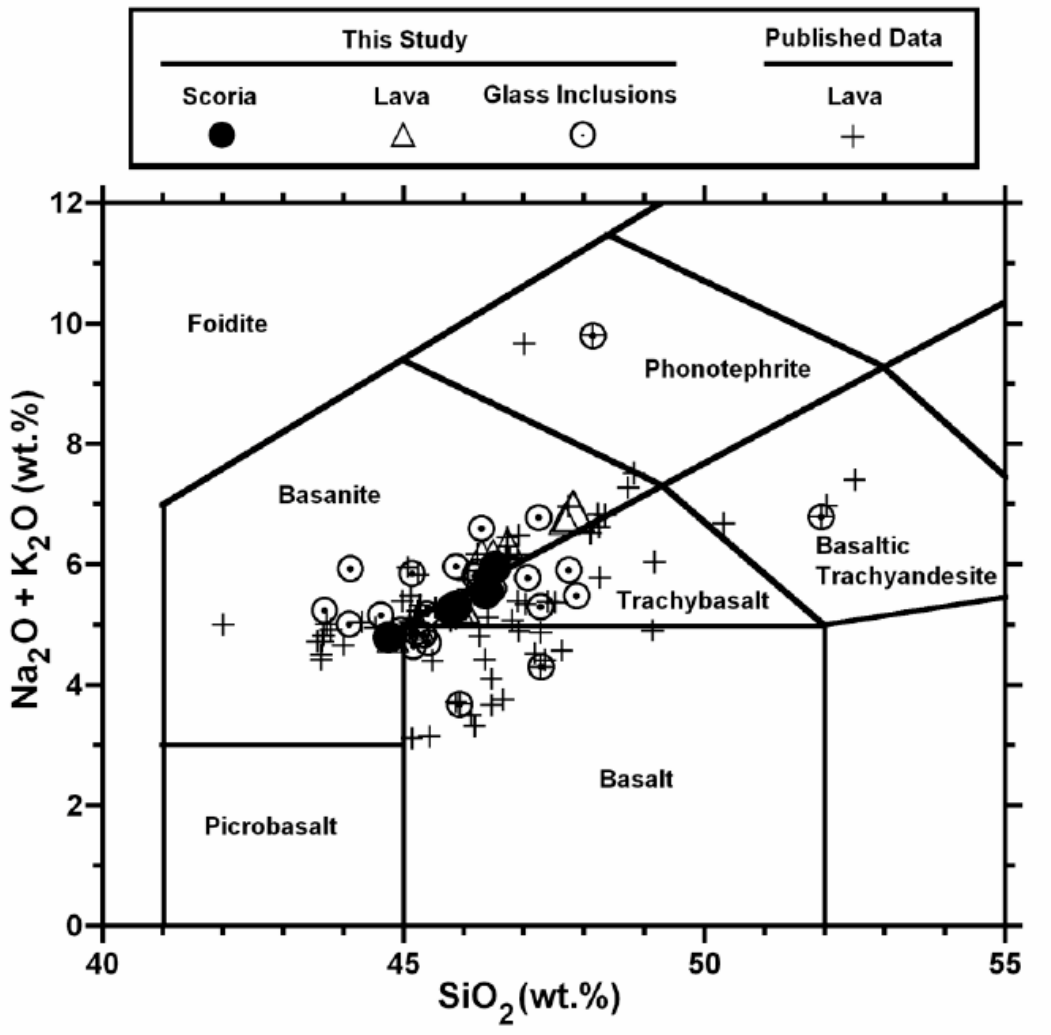

Suh et al. – Fig. 3

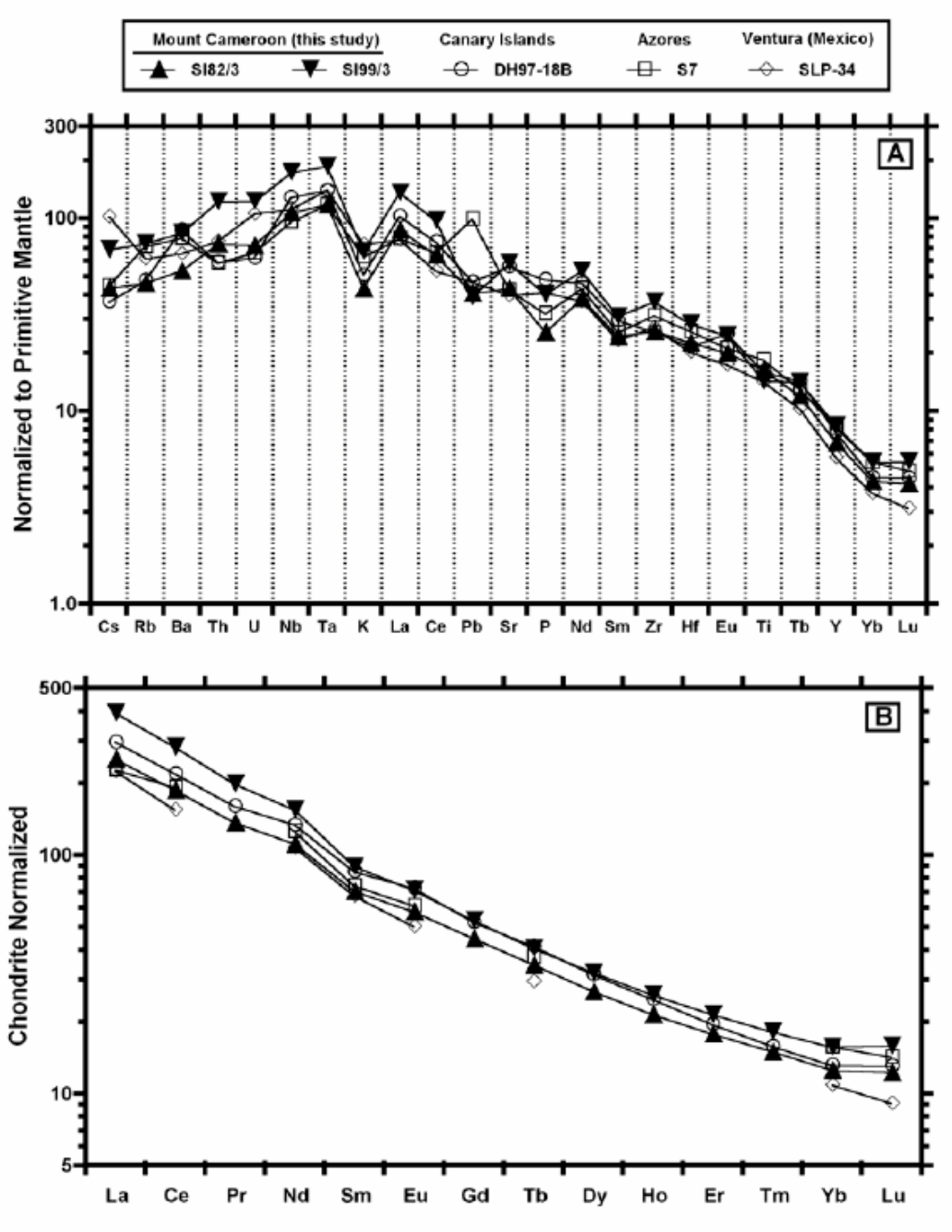

Suh et al. – Fig. 4

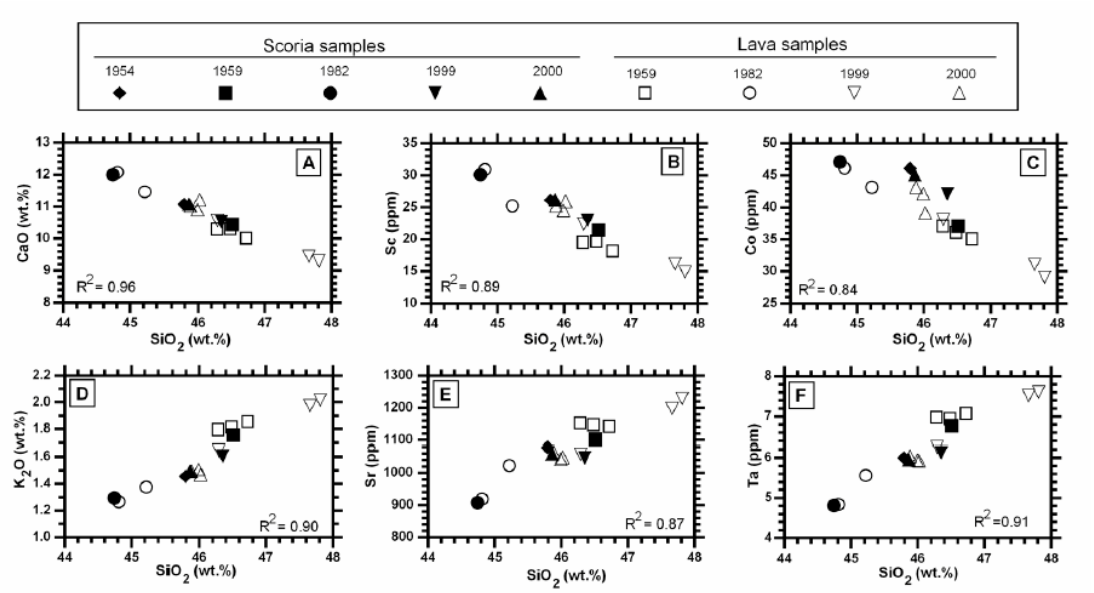

Suh et al. – Fig. 5

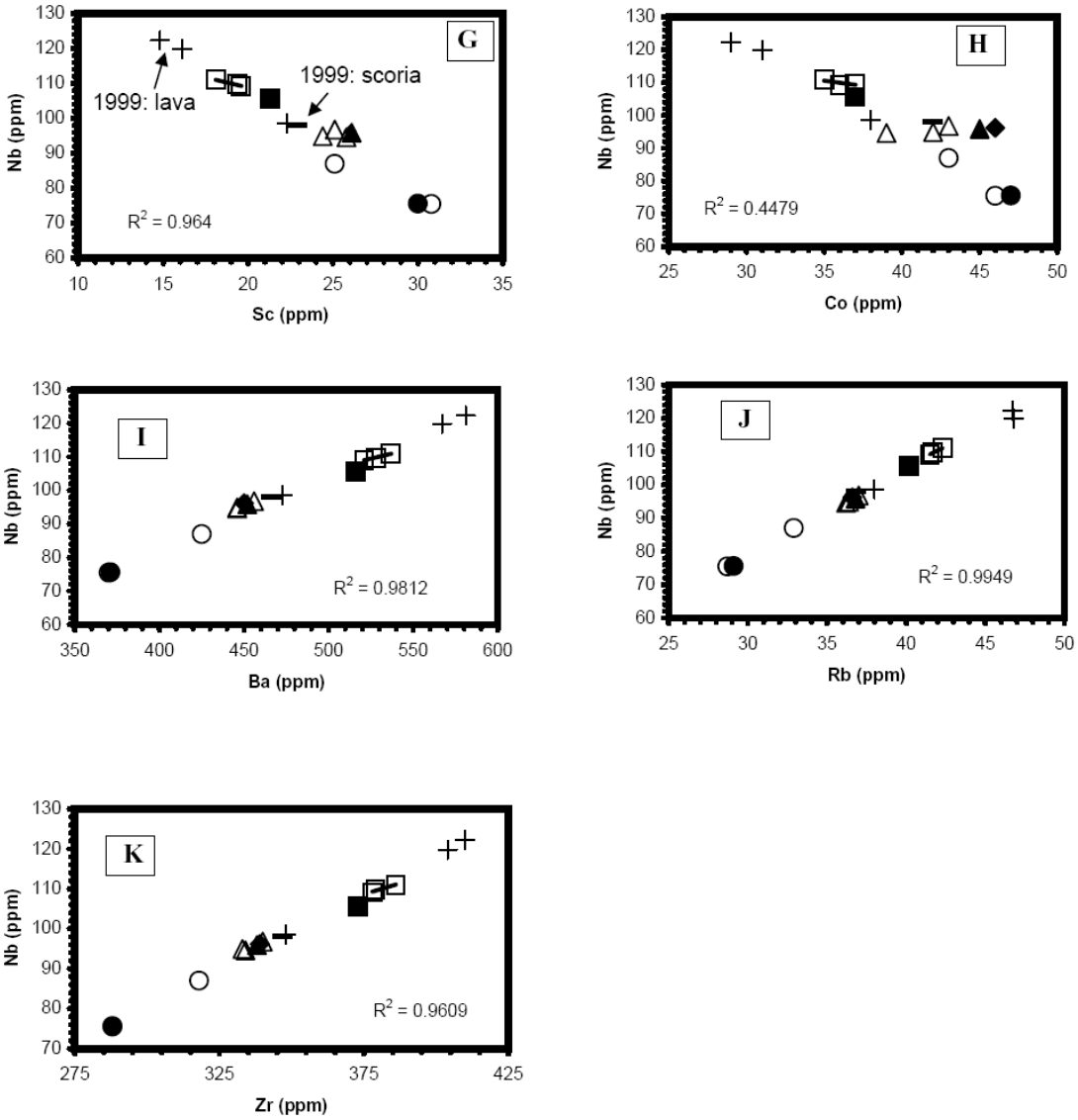

Suh et al. - Fig. 5 (continued)

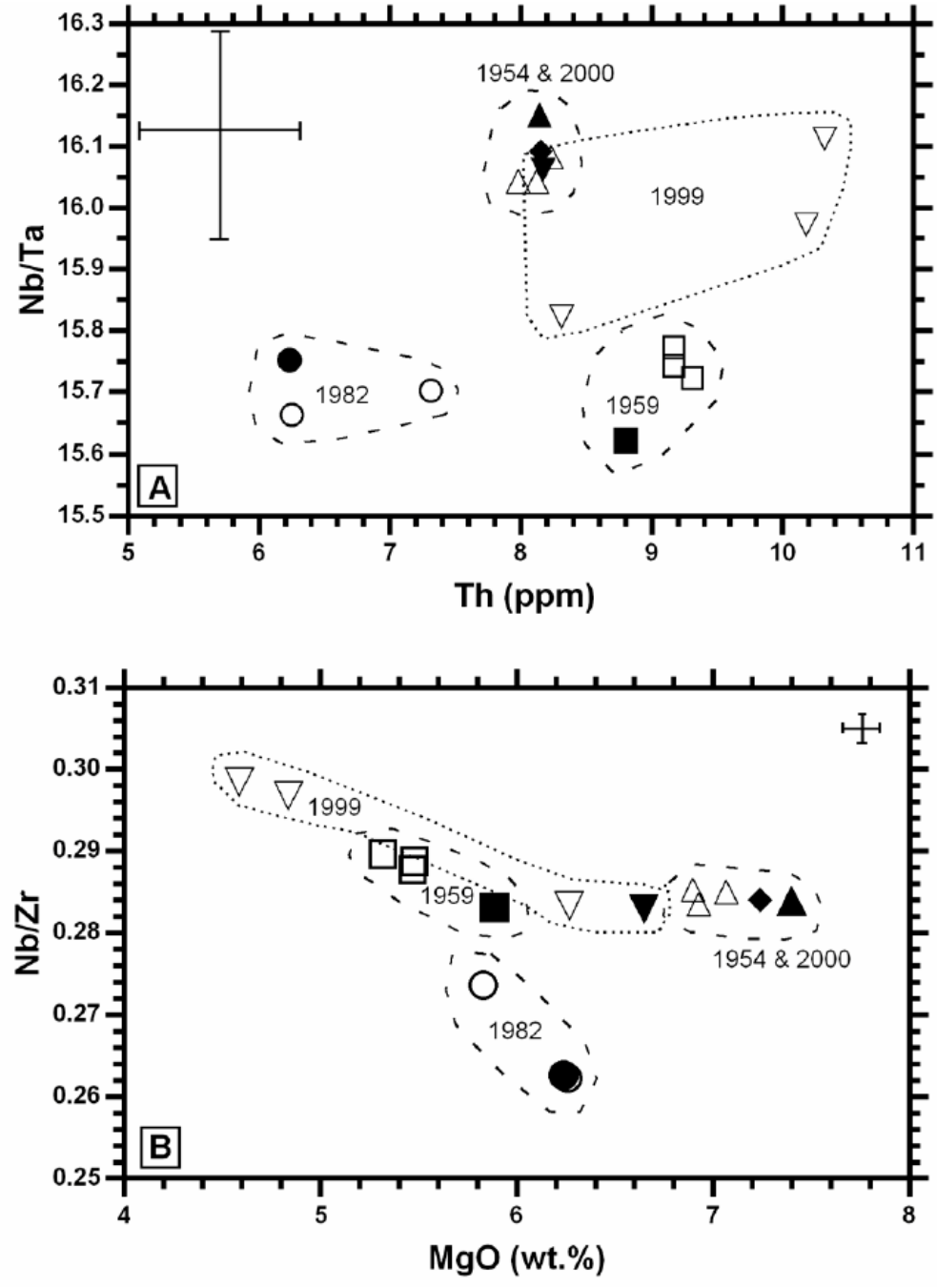

Suh et al. – Fig. 6

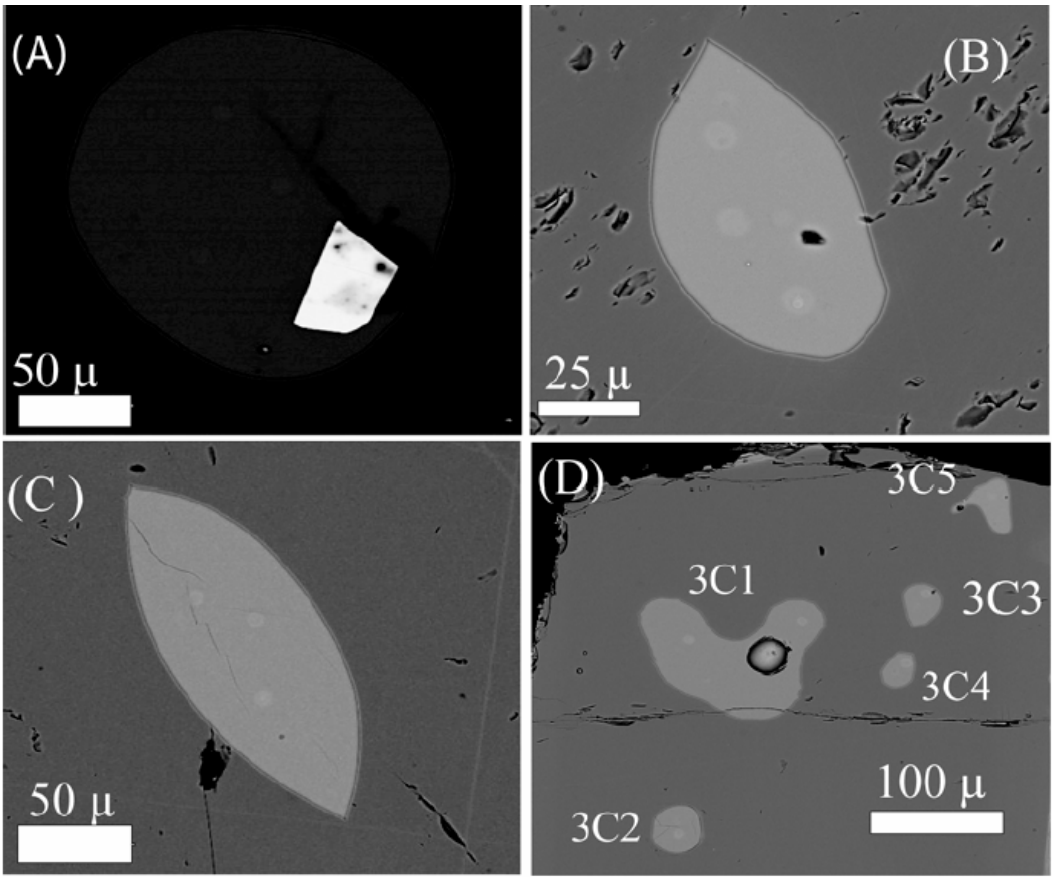

Suh et al. – Fig. 7

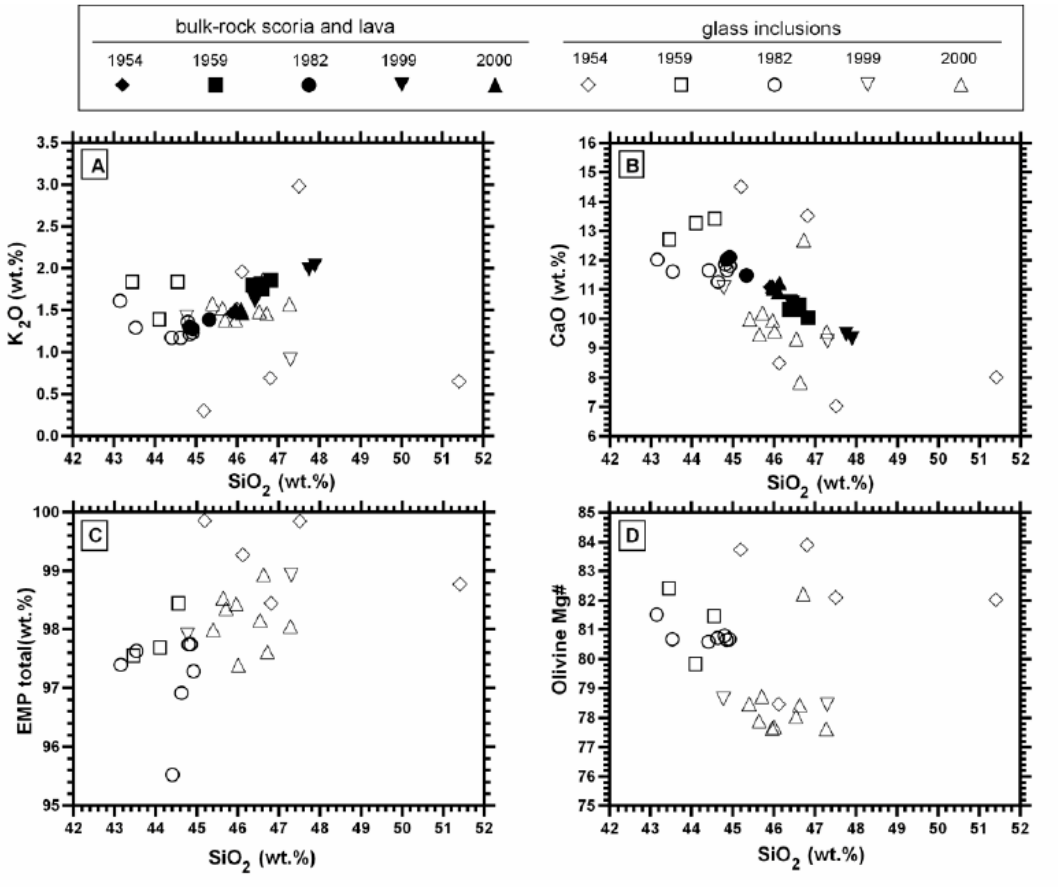

Suh et al. – Fig. 8

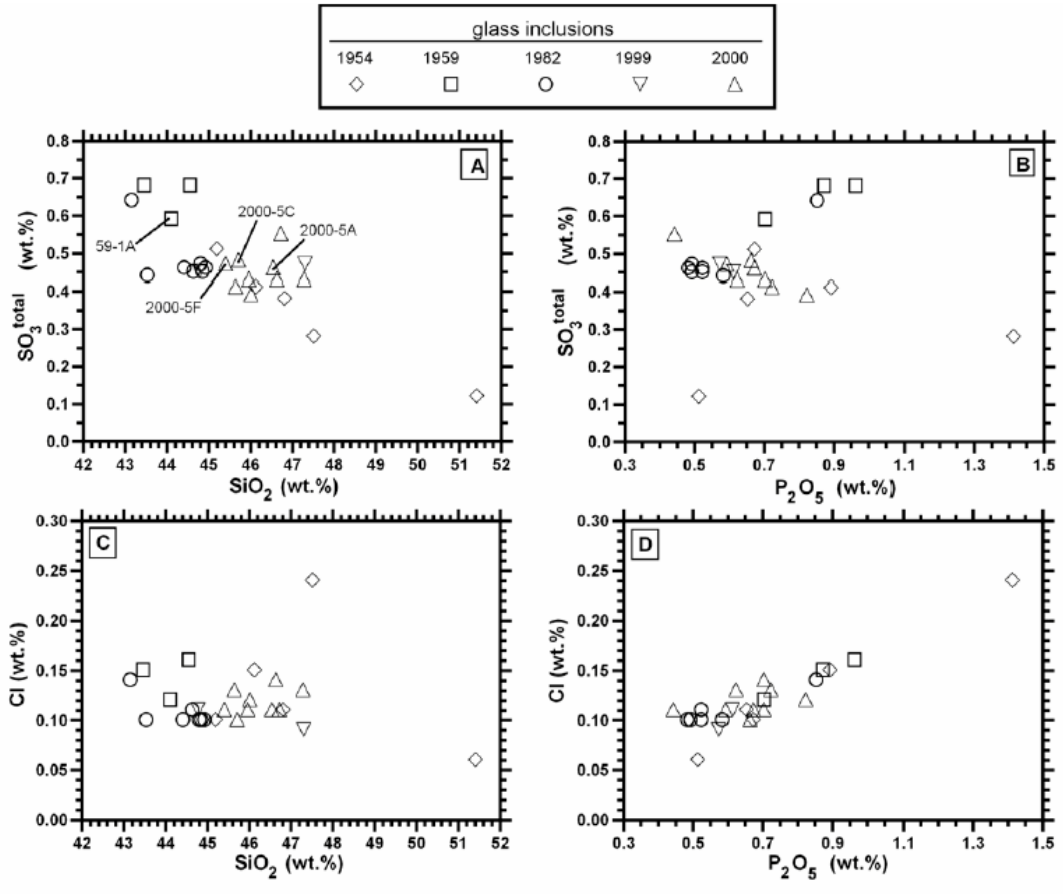

Suh et al. – Fig. 9

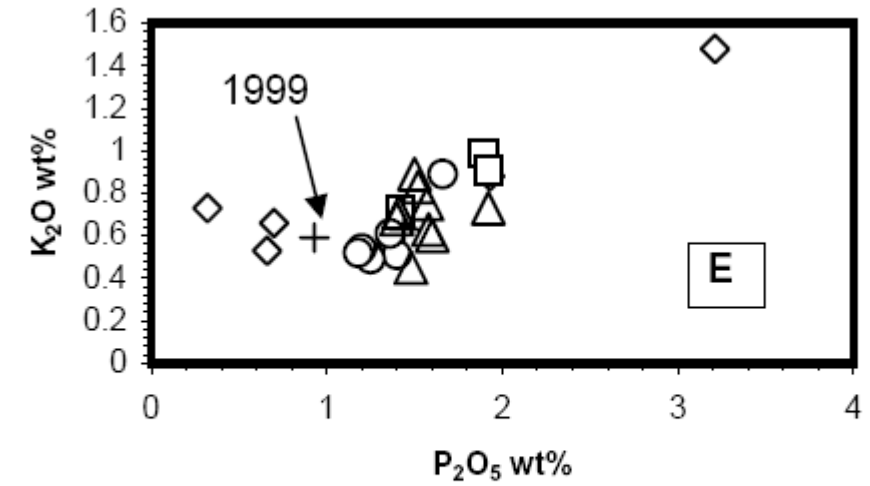

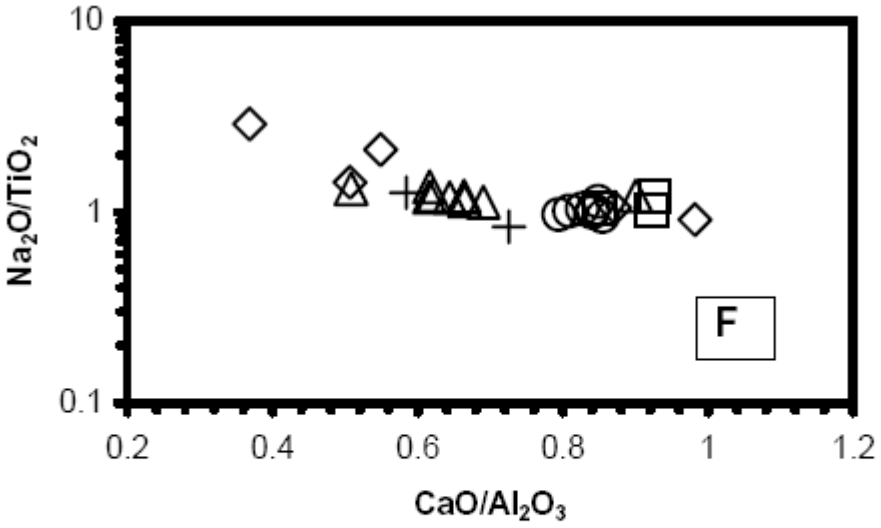

Suh et al. - Fig. 9 (continued)

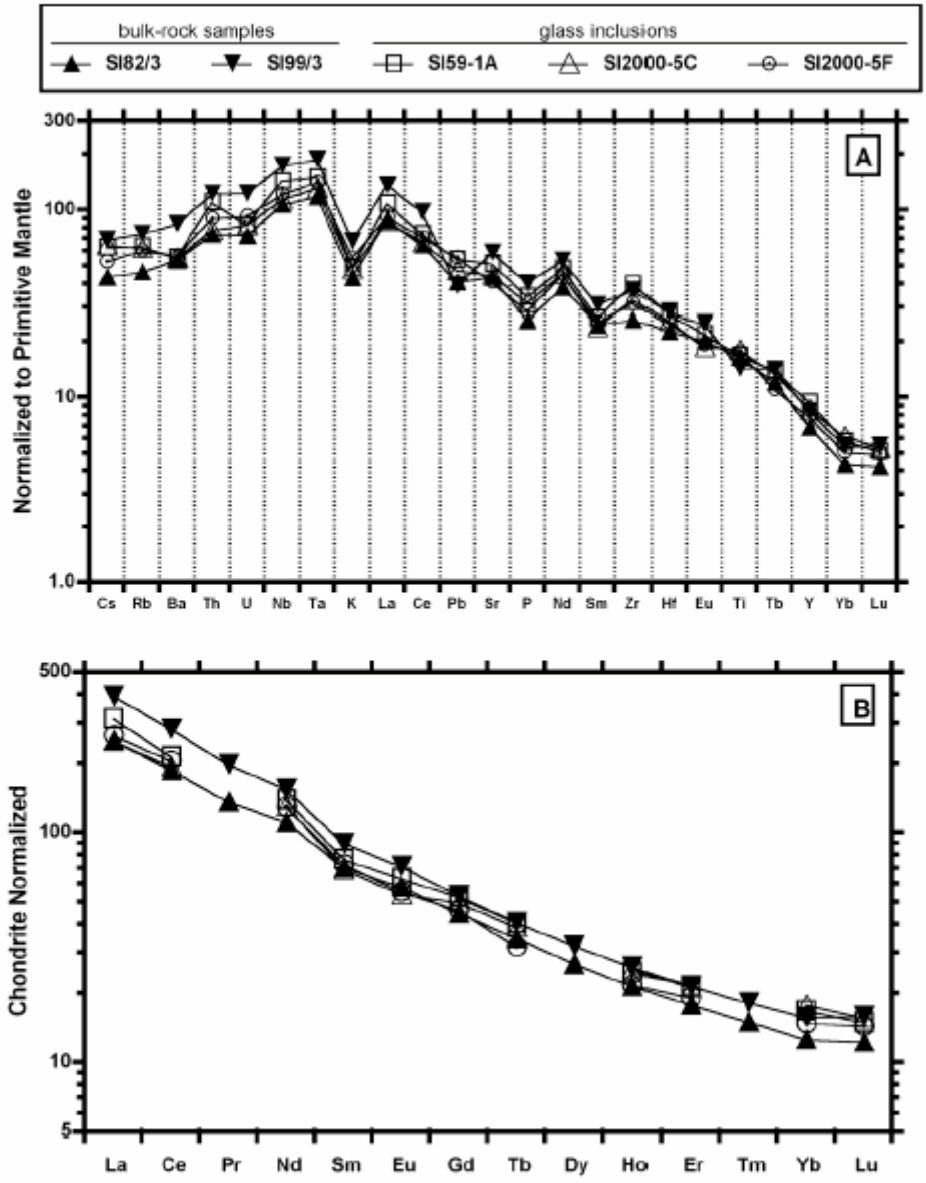

Suh et al. – Fig. 10

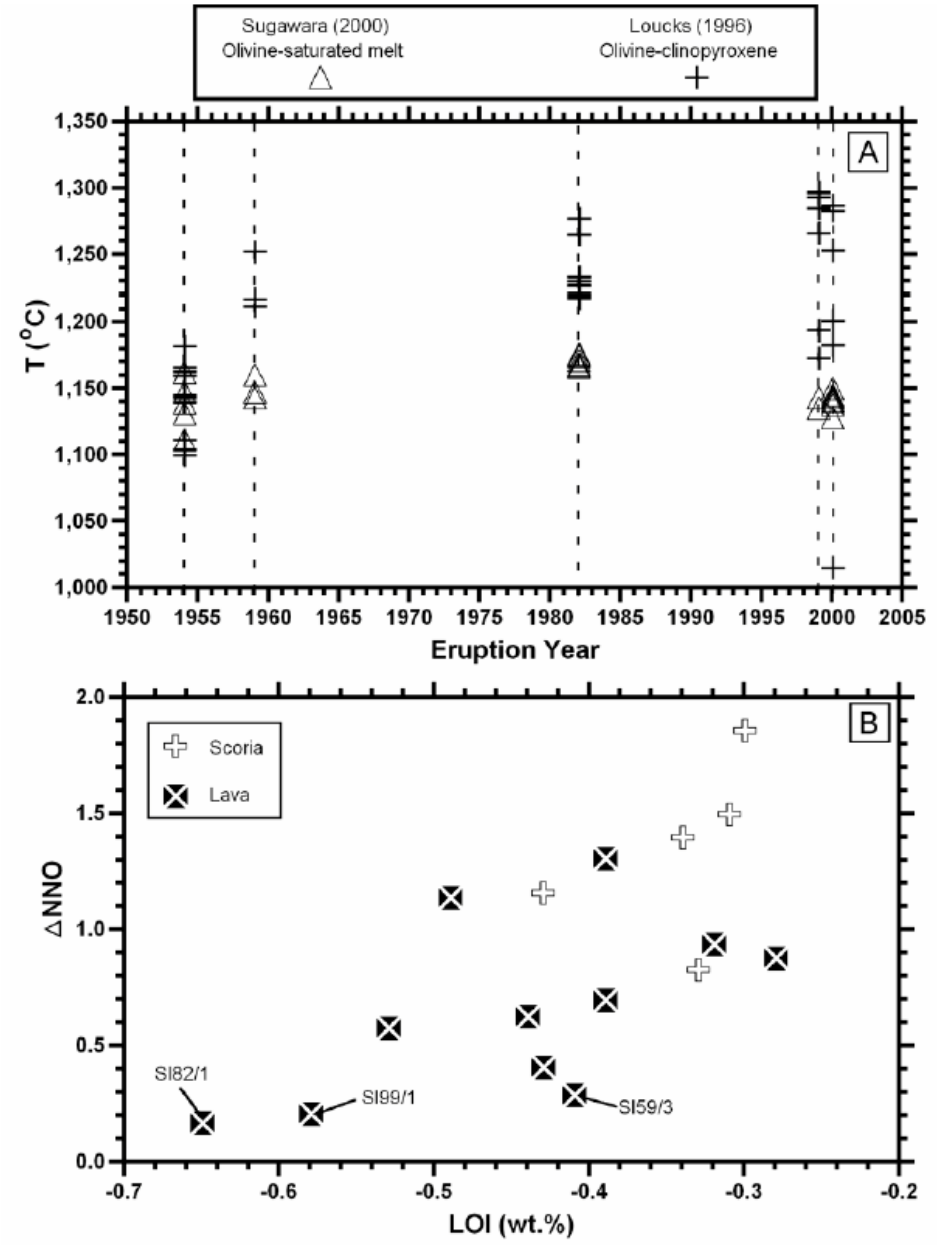

Suh et al. – Fig. 11

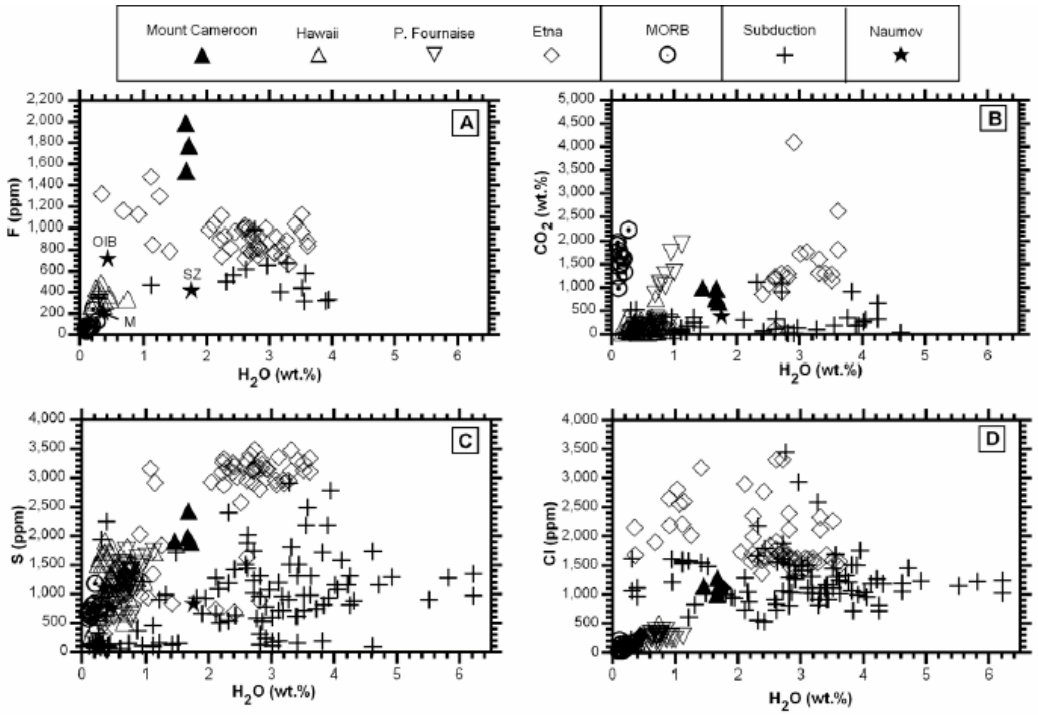

Suh et al. – Fig. 12